Chapter 12
CDMA Cellular Systems

CDMA has been adopted in third generation (3G) cellular systems, notably in the cdma2000 and WCDMA standards, due to its many benefits such as universal frequency reuse, soft handoff capability, and the ability to exploit multipath fading with RAKE receivers. CDMA waveforms are broadband and noise-like, so that the multiple-access interference behaves in a manner that is approximately equivalent to additional AWGN. CDMA cellular systems are interference limited and, therefore, their capacities are closely related to the amount of multiple-access interference that is generated by the transmitters on one hand and tolerated by the receivers on the other. Because of the universal frequency reuse, multiple-access interference in CDMA cellular systems is due to both intra-cell interference from transmissions in the same cell and inter-cell interference from transmissions in neighboring cells. To alleviate the level of multiple-access interference, and thus increase the capacity and quality, CDMA systems must use power control in conjunction with soft handoff. The fundamental idea behind power control is to limit the generation of multiple-access interference by restraining mobile stations (MSs) and base stations (BSs) from transmitting any more power than is necessary. With power control, each MS and BS transmits just enough power to meet the required carrier-to-interference ratio (CIR) at the intended receiver.

This chapter considers capacity and performance of CDMA cellular systems. Section 12.1 begins the chapter with a discussion of the power control mechanism in the CDMA reverse and forward links. We then consider the reverse and forward link capacity of CDMA cellular systems, and demonstrate the impact of imperfect power control in Sect. 12.2. Section 12.3 considers hierarchical CDMA cellular architectures consisting of macrocells and underlaid macrocells, where both hierarchical layers use the entire system bandwidth. On the reverse link, this is accomplished using Macrodiversity maximal ratio combining (MMRC) where the signals received at multiple BSs are coherently combined. On the forward link, only one BS can transmit to a given MS at any given time. The forward link transmit power is determined according to a neighboring cell pilot power scheme, where

G.L. Stüber, *Principles of Mobile Communication*, DOI 10.1007/978-1-4614-0364-7_12,

the forward transmit power to each MS is determined according to link conditions between the MS and surrounding BSs. It is also shown that some improvement can be gained using selective transmit diversity at the BSs on the forward link.

12.1 CDMA Power Control

CDMA cellular systems must use reverse channel power control to combat the near-far effect, a phenomenon where the signals received from distant MSs will experience excessive multiple-access interference from close-in MSs due to differences in the propagation path loss. Shadowing and envelope fading will also contribute significantly to the near-far effect, although these propagation factors are not distance dependent. To combat variations in the received CIR due to path loss, shadowing and envelope fading, the reverse link in CDMA cellular systems uses a fast closed-loop power control algorithm. For cdma2000 cellular systems, the transmit power from each MS is adjusted every 1.25 ms to equalize the corresponding received CIR at the serving BS. Such adjustments are based on measurements of the received E_b/N_t (bit energy to interference-plus-noise spectral density ratio). The reverse closed-loop power control algorithm consists of outer and inner power control loops. The outer power control loop occurs between the base station controller and the BSs, and adjusts a "set point" or target received E_b/N_t according to measurements of the frame error rate that is required to maintain a desired quality of service. The outer loop adjustments are performed at the frame interval, for example, every 20 ms in cdma2000. The inner power control loop occurs between the BSs and MSs. The serving BS compares measurements of the received E_b/N_t from each MS to the corresponding target E_b/N_t. Based on the results of these comparisons the BS instructs each MS to either increase or decrease its transmit power by a power increment at short periodic intervals, for example, ± 1 dB every 1.25 ms in cdma2000.

CDMA cellular systems also use forward link power control to combat the corner effect, a condition where an MS experiences a decrease in received CIR near the corner of a cell. While the IS-95A/B cellular system uses open-loop power control on the forward link, 3G CDMA cellular systems such as cdma2000 and WCDMA also use fast closed-loop power control on the forward link based on measurements of the received E_c/I_o (chip energy to interference-plus-noise spectral density ratio) that are obtained from the forward pilot channel. Once again, the forward closed-loop power control algorithm consists of outer and inner power control loops. The outer power control loop is carried out entirely within the MS, where the MS adjusts a "set point" or target received E_c/I_o according to measurements of the frame error rate that is required to maintain a desired quality of service. The outer loop adjustments can be performed at the frame interval, for example, every 20 ms in cdma2000. The inner power control loop occurs between the MSs and BSs. The MS compares measurements of the received E_c/I_o from the BS to the corresponding

target E_c/I_o. Based on the results of these comparisons, the MS instructs the BS to either increase or decrease its transmit power by a predetermined power increment at short periodic intervals, for example, ± 1 dB every 1.25 ms in cdma2000.

The basic idea of CDMA power control can be described as follows [150, 254]. We consider the CDMA reverse link where a BS serves K MSs (although the same argument can be applied to forward link power control). The reverse link CIR experienced by MS i, $(C/I)_i$, is

$$(C/I)_i = \frac{G_i P_i}{\sum_{\substack{j=1 \\ j\neq i}}^{K} G_j P_j + I_o + N_o}, \tag{12.1}$$

where G_i is the link gain (due to path loss, shadowing, and fading) between MS_i and the BS, and P_i is the reverse transmit power MS_i. The term I_o represents the out-of-cell interference generated by the surrounding cells and N_o is the additive white Gaussian noise (AWGN). The goal is to develop a recursive algorithm to adjust the transmit power of MS_i to drive $(C/I)_i$ to meet or exceed a desired target value, $(C/I)_{\text{target},i}$, that is, we wish to have

$$(C/I)_i \geq (C/I)_{\text{target},i}\ , \quad i \leq i \leq K. \tag{12.2}$$

Rearranging (12.1) gives

$$P_i = \sum_{\substack{j=1 \\ j\neq i}}^{K} (C/I)_i \frac{G_j}{G_i} P_j + (C/I)_i \frac{I_o + N_o}{G_i}. \tag{12.3}$$

Based on the above derivation, we define a $K \times K$ matrix $\mathbf{W} = [W_{ij}]$ and a vector $\mathbf{U} = (U_i)$ having elements

$$W_{ij} = \begin{cases} 1, & , \ i = j, \\ -(C/I)_{\text{target},i} \frac{G_j}{G_i}\ , & i \neq j, \end{cases} \tag{12.4}$$

$$U_i = (C/I)_{\text{target},i} \frac{I_o + N_o}{G_i}\ , \quad 1 \leq i \leq K. \tag{12.5}$$

The existence of a power vector, $\mathbf{P} = (P_1, P_2, \ldots, P_K)^T$, such that $\mathbf{WP} = \mathbf{U}$ implies that $(C/I)_i \geq (C/I)_{\text{target},i}, 1 \leq i \leq K$. When such a matrix $\mathbf{P}$ exists, $\mathbf{W}$ has only strictly positive eigenvalues and, therefore, $\mathbf{P}$ is given by

$$\mathbf{P} = \mathbf{W}^{-1}\mathbf{U}. \tag{12.6}$$

It is proven in [254] that whenever a unique power vector $\mathbf{P}$ satisfying $(C/I)_{\text{target},i}$, $1 \leq i \leq K$, exists, $\mathbf{P}(n)$ converges to $\mathbf{P} = \mathbf{W}^{-1}\mathbf{U}$ for any initial power vector $\mathbf{P}(0)$ according to the following recursion:

$$\mathbf{P}(n+1) = (\mathbf{I} - \mathbf{W})\mathbf{P}(n) + \mathbf{U}. \tag{12.7}$$

The above recursion can be rewritten as

$$P_i(n+1) = P_i(n)\frac{(C/I)_{\text{target},i}}{(C/I)_i(n)}, \tag{12.8}$$

where $P_i(n)$ and $(C/I)_i(n)$ are the transmit power of MS_i and $(C/I)_i$ at step n, respectively.

12.2 Capacity of Cellular CDMA

Numerous studies have investigated the capacity and performance of CDMA cellular systems for radio propagation environments characterized by path loss and shadowing, including Gilhousen et al. [110], Kudoh and Matsumoto [145], and Newson and Heath [194]. Mokhtar and Gupta [182] considered reverse channel capacity on shadowed Nakagami fading channels, where the desired and interfering signals have the same statistical fading characteristics.

CDMA cellular systems use universal frequency reuse, where the bandwidth is shared by all the cells and users are distinguished through the assignment of unique spreading sequences. For such systems, multiple-access interference from both in-cell and out-of-cell sources must be carefully accounted for. The propagation path loss associated with out-of-cell interferers is relatively small due to the short reuse distance and, hence, the associated interference is significant. With cellular CDMA systems, any technique that reduces or mitigates multiple-access interference translates directly into a capacity gain. For this reason CDMA systems use voice activity detection along with variable rate speech coding, where the rate of the speech coder is reduced when silent periods are detected in the speech waveform.

Our analysis of cellular CDMA capacity assumes a uniform plane of hexagonal cells of radius R. Each cell contains a centrally located BS with 120^{o} cell sectors. It is further assumed that the MSs are uniformly distributed throughout the system area with a density of K MSs per cell sector. For hexagonal cells of radius R, this yields a subscriber density of

$$\rho = \frac{2K}{3\sqrt{3}R^2} \text{ per unit area.} \tag{12.9}$$

The effects of variable rate speech coding can be modeled by assuming that each transmitter is independently active at any time with probability p, so that the number of active transmitters in each cell has a (K, p) binomial distribution. The average number of active transmitters in a cell sector is Kp.

12.2.1 Reverse Link Capacity

Our analysis assumes a simple closed-loop reverse channel power control scheme that equalizes the received power C at a BS from all MSs being served by that BS. Let $\mathrm{MS}_{i,j}$ denote the jth MS located in cell i. The power transmitted by $\mathrm{MS}_{i,j}$, located at distance $d_{i,j}$ from its serving BS, BS_i, is $P_{i,j}$. The received power at BS_i is

$$C = P_{i,j} 10^{\frac{\varsigma_{i,j}}{10}}, \tag{12.10}$$

where $\varsigma_{i,j}$ is a random gain (in decibel units) due to path loss, shadowing and fading. $\mathrm{MS}_{i,j}$ is also located at distance $d_{i,0}$ to the reference BS, BS_0, and will produce an out-of-cell interference equal to

$$\begin{aligned} \frac{I_{\mathrm{o}}(i,j)}{C} &= 10^{\varsigma_{i,0}/10} \cdot \left(\frac{1}{10^{\varsigma_{i,j}/10}} \right) \\ &= 10^{(\varsigma_{i,0} - \varsigma_{i,j})/10} \leq 1. \end{aligned} \tag{12.11}$$

The first term is due to path loss, shadowing and fading to BS_0, while the second term is the effect of the power control to compensate for the random attenuation between $\mathrm{MS}_{i,j}$ and BS_j. Note that $I_{\mathrm{o}}(i,j)/C$ is always less than unity; otherwise the MS will execute a handoff to another BS that will make it less than unity.

For our purpose, we assume log-normal shadowing with Nakagami fading, where the received squared-envelope has the composite *Gamma*-log-normal pdf in (2.313). The composite *Gamma*-log-normal pdf can be approximated by a purely log-normal pdf with mean and standard deviation given by (2.314). Hence, the random variables $\varsigma_{i,j}$ and $\varsigma_{i,0}$ are treated as Gaussian random variables with means and variances, respectively,

$$\begin{aligned} \mu_{i,j\ (\mathrm{dBm})} &= \xi^{-1}(\psi(m_{i,j}) - \ln(m_{i,j})) + \mu_{\Omega_{\mathrm{p}\ (\mathrm{dBm})}}(i,j), \\ \mu_{i,0\ (\mathrm{dBm})} &= \xi^{-1}(\psi(m_{i,0}) - \ln(m_{i,0})) + \mu_{\Omega_{\mathrm{p}\ (\mathrm{dBm})}}(i,0), \\ \sigma_{i,j}^2 &= \xi^{-2}\zeta(2, m_{i,j}) + \sigma_{\Omega}^2, \\ \sigma_{i,0}^2 &= \xi^{-2}\zeta(2, m_{i,0}) + \sigma_{\Omega}^2, \end{aligned} \tag{12.12}$$

where $\xi = \ln(10)/10$, $m_{i,j}$ and $m_{i,0}$ are the Nakagami shape factors, and σ_{Ω} is the shadow standard deviation. The parameters $\mu_{\Omega_{\mathrm{p}\ (\mathrm{dBm})}}(i,j)$ and $\mu_{\Omega_{\mathrm{p}\ (\mathrm{dBm})}}(i,0)$ are determined by the path loss. Using the simple path loss model in (1.5), their difference is

$$\mu_{\Omega_{\mathrm{p}\ (\mathrm{dBm})}}(i,j) - \mu_{\Omega_{\mathrm{p}\ (\mathrm{dBm})}}(i,0) = 10\beta \log_{10}\left\{ d_{i,j}/d_{i,0} \right\}. \tag{12.13}$$

The total out-of-cell interference-to-signal ratio is equal to

$$\frac{I_{\mathrm{o}}}{C} = \int\int \chi I_{\mathrm{o}}(i,j)\Phi_{0,j}\rho \mathrm{d}A, \tag{12.14}$$

where

$$\Phi_{0,j} = \begin{cases} 1, & \text{if } \ 10^{(\varsigma_{i,0}-\varsigma_{i,j})/10} < 1 \\ 0, & \text{otherwise} \end{cases}, \tag{12.15}$$

ρ is user density over the area A, and χ is the voice activity variable

$$\chi = \begin{cases} 1\,, & \text{with probability} \quad p. \\ 0\,, & \text{with probability} \quad 1-p \end{cases}. \tag{12.16}$$

The total out-of-cell interference I_{o} can be modeled as a Gaussian random variable by invoking the central limit theorem. The mean of the total out-of-cell interference-to-carrier ratio is

$$\begin{aligned} \mathrm{E}[I_{\mathrm{o}}/C] &= \int\int \mathrm{E}[\chi 10^{(\varsigma_{i,0}-\varsigma_{i,j})/10}\Phi_{0,j}]\rho \mathrm{d}A \\ &= \int\int p\mathrm{E}[10^{(\varsigma_{i,0}-\varsigma_{i,j})/10}\Phi_{0,j}]\rho \mathrm{d}A. \end{aligned} \tag{12.17}$$

Let $x = \varsigma_{i,0} - \varsigma_{i,j}$ and define

$$\begin{aligned} \mu_{x\ (\mathrm{dB})} &= \mu_{i,0\ (\mathrm{dBm})} - \mu_{i,j\ (\mathrm{dBm})}, \\ \sigma_x^2 &= \sigma_{i,0}^2 + \sigma_{i,j}^2. \end{aligned} \tag{12.18}$$

The expectation in the integrand of (12.17) is

$$\begin{aligned} \mathrm{E}[10^{(\varsigma_{i,0}-\varsigma_{i,j})/10}\Phi_{0,j}] &= \int_{-\infty}^{0} \mathrm{e}^{\xi x} \frac{1}{\sqrt{2\pi}\sigma_x} \exp\left\{ -\frac{(x-\mu_{x\ (\mathrm{dB})})^2}{2\sigma_x^2} \right\} \mathrm{d}x \\ &= \exp\left\{ \frac{\xi^2\sigma_x^2}{2} + \xi\mu_{x\ (\mathrm{dB})} \right\} \frac{1}{\sqrt{2\pi}\sigma_x} \\ &\quad \times \int_{-\infty}^{0} \exp\left\{ -\left(\frac{x}{\sqrt{2}\sigma_x} - \frac{\xi\sigma_x}{\sqrt{2}} - \frac{\mu_{x\ (\mathrm{dB})}}{\sqrt{2}\sigma_x} \right)^2 \right\} \mathrm{d}x \\ &= \exp\left\{ \frac{\xi^2\sigma_x^2}{2} + \xi\mu_{x\ (\mathrm{dB})} \right\} \left(1 - Q\left(-\xi\sigma_x - \frac{\mu_{x\ (\mathrm{dB})}}{\sigma_x} \right) \right). \end{aligned} \tag{12.19}$$

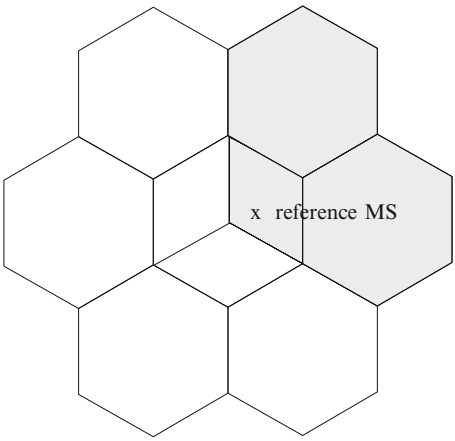

Fig. 12.1 Reverse channel transmissions from MSs located in the shaded area will cause out-of-cell interference with the reverse channel transmission from the reference MS

Therefore,

$$\mathrm{E}[I_{\mathrm{o}}/C] = p\int\int \exp\left\{\frac{\xi^2\sigma_x^2}{2} + \xi\mu_{x\,(\mathrm{dB})}\right\}\left(1 - Q\left(-\xi\sigma_x - \frac{\mu_{x\,(\mathrm{dB})}}{\sigma_x}\right)\right)\rho\,\mathrm{d}A. \tag{12.20}$$

In a similar fashion,

$$\begin{aligned}\mathrm{E}[(I_{\mathrm{o}}/C)^2] &= \int\int \mathrm{E}[\chi^2 10^{(\varsigma_{i0}-\varsigma_{ij})/5}\Phi_{0,j}^2]\rho\,\mathrm{d}A \\ &= p\int\int\int_{-\infty}^{0} \mathrm{e}^{2\xi x}\frac{1}{\sqrt{2\pi}\sigma_x}\exp\left\{-\frac{(x-\mu_{x\,(\mathrm{dB})})^2}{2\sigma_x^2}\right\}\mathrm{d}x\rho\,\mathrm{d}A \\ &= p\int\int \exp\left\{2\xi^2\sigma_x^2 + 2\xi\mu_{x\,(\mathrm{dB})}\right\}\left(1 - Q\left(-2\xi\sigma_x - \frac{\mu_{x\,(\mathrm{dB})}}{\sigma_x}\right)\right)\rho\,\mathrm{d}A.\end{aligned} \tag{12.21}$$

Finally, the variance of I_{o}/C is

$$\begin{aligned}\mathrm{Var}[I_{\mathrm{o}}/C] = p\int\int \exp\left\{2\xi^2\sigma_x^2 + 2\xi\mu_{x\,(\mathrm{dB})}\right\}\left(1 - Q\left(-2\xi\sigma_x - \frac{\mu_{x\,(\mathrm{dB})}}{\sigma_x}\right)\right)\rho\,\mathrm{d}A \\ -\mathrm{E}^2[I_{\mathrm{o}}/C].\end{aligned} \tag{12.22}$$

The integrals in (12.20) and (12.22) must be evaluated numerically over the random location of mobile locations in the area A, as defined by the set of shaded sectors shown in Fig. 12.1 (minus the sector where the reference MS is located) where only the adjacent cells are shown.

With perfect power control, the in-cell interference I_{in} is

$$I_{\text{in}} = C \sum_{i=1}^{K-1} \chi_i, \tag{12.23}$$

where χ_i is a Bernoulli random variable equal to 1 with probability p and 0 with probability $1-p$. Let $I = I_{\text{o}} + I_{\text{in}}$ be the total interference. The CIR C/I and baseband $E_{\text{b}}/N_{\text{o}}$ are related by

$$C/I = \frac{E_{\text{b}}/N_{\text{o}}}{W_{\text{ss}}/W}, \tag{12.24}$$

where E_{b} is bit energy, N_{o} the one-sided noise power spectral density, W_{ss} the spread spectrum bandwidth, and W is the data signal bandwidth. Many factors must be considered to establish the required $\gamma_{\text{b}} = E_{\text{b}}/N_{\text{o}}$, denoted by $\gamma_{\text{b req}}$, such as the channel characteristics, type of modulation, diversity, receiver structure, and coding/interleaving techniques. In the cdma2000 cellular system with radio configuration (RC1), $\gamma_{\text{b req}} = 7\,\text{dB}$ on the reverse link and $\gamma_{\text{b req}} = 5\,\text{dB}$ on the forward link [110]. The difference in $\gamma_{\text{b req}}$ for the forward and reverse links arises, because the reverse link of cdma2000 RC1 uses noncoherent detection while the forward link uses coherent detection.

From (12.24), we can write

$$(I/C)_{\gamma_{\text{b}}} = \frac{W_{\text{ss}}/W}{\gamma_{\text{b}}}. \tag{12.25}$$

It follows that the probability that the received γ_{b} at a BS is below a required value, $\gamma_{\text{b req}}$, is

$$\begin{aligned}
P_{\text{out}} &= \text{P}[\gamma_{\text{b}} < \gamma_{\text{b req}}] \\
&= \text{P}[(I/C)_{\gamma_{\text{b}}} > (I/C)_{\gamma_{\text{b req}}}] \\
&= \text{P}\left[\sum_{i=1}^{K-1} \chi_i + I_{\text{o}}/C > (I/C)_{\gamma_{\text{b req}}}\right] \\
&= \text{P}\left[I_{\text{o}}/C > (I/C)_{\gamma_{\text{b req}}} - \sum_{i=1}^{K-1} \chi_i\right] \\
&= \sum_{k=0}^{K-1} \text{P}\left[I_{\text{o}}/C > (I/C)_{\gamma_{\text{b req}}} - k \,\middle|\, \sum_{i=1}^{K-1} \chi_i = k\right] \text{P}\left[\sum_{i=1}^{K-1} \chi_i = k\right] \\
&= \sum_{k=0}^{K-1} \binom{K-1}{k} p^k (1-p)^{K-1-k} Q\left(\frac{(I/C)_{\gamma_{\text{b req}}} - k - \text{E}[I_{\text{o}}/C]}{\sqrt{\text{Var}[I_{\text{o}}/C]}}\right).
\end{aligned} \tag{12.26}$$

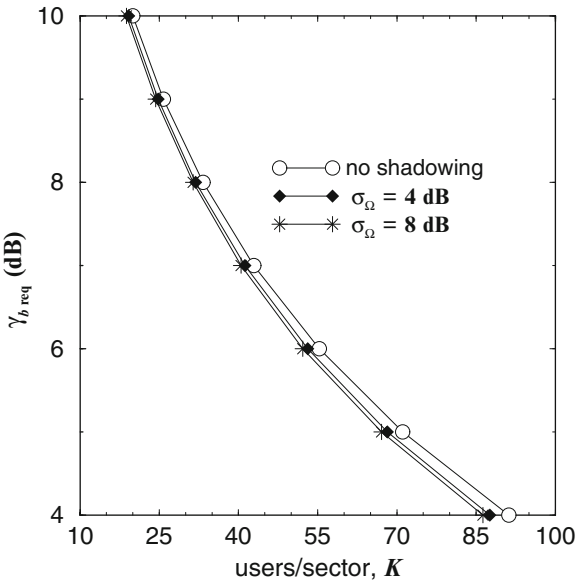

Fig. 12.2 Reverse channel capacity with $P_{\text{out}} = 10^{-2}$ for different $\gamma_{\text{b req}}$; the Nakagami shape factors are $m_{\text{d}} = 1$ and $m_{\text{I}} = 1$ (Rayleigh fading), and σ_Ω is the shadow standard deviation

We assume a chip rate of $W_{\text{ss}} = 1.25\,\text{MHz}$, $W = 8\,\text{kHz}$, $p = 3/8$, and a required outage probability of $P_{\text{out}} = 10^{-2}$. Figure 12.2 shows the reverse channel capacity for different $\gamma_{\text{b req}}$ and shadow standard deviations. The reverse channel capacity is greatly increased by a reduction in $\gamma_{\text{b req}}$ and is slightly reduced when the shadow standard deviation is increased. Figure 12.3 shows the reverse channel capacity with different Nakagami shape factors for the desired and interfering signals. Observe that a change in the Nakagami shape factor m_{I} of interfering signals has very little effect on the reverse channel capacity. Figure 12.4 further illustrates the effect of fading and shadowing on the reverse channel capacity. As expected, shadowing and fading have relatively little impact on the reverse channel capacity, since these components of the received signal are power controlled. Therefore, fading and shadowing variations mostly affect the out-of-cell interference.

The ratio of the mean out-of-cell interference to the mean in-cell interference is

$$\theta = \frac{\text{E}[I_{\text{o}}]}{\text{E}[I_{\text{in}}]} = \frac{\text{E}[I_{\text{o}}/C]}{\text{E}[I_{\text{in}}/C]} = \frac{\text{E}[I_{\text{o}}/C]}{pK}. \tag{12.27}$$

With a fourth-order path loss exponent, Newson and Heath [194] showed that $\theta = 0.5$ when no fading and shadowing are considered and $\theta \approx 0.66$ when shadowing is considered with $\sigma_\Omega = 8\,\text{dB}$. This translates into a frequency reuse efficiency f, defined as the ratio of mean in-cell interference to the total mean interference, of 0.66 and 0.38, respectively. Table 12.1 tabulates the corresponding values of θ and $f = 1/(1+\theta)$ for different propagation conditions. The calculations only

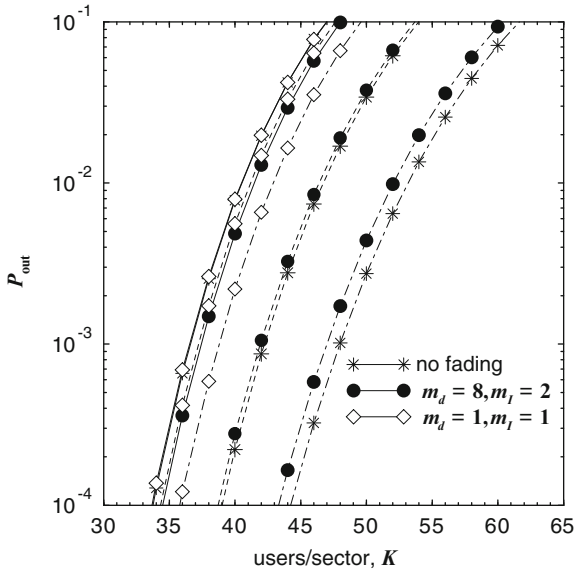

Fig. 12.3 Reverse channel capacity for different propagation environments with $\gamma_{b\ req} = 7$ dB. *Solid lines* denote $\sigma_\Omega = 0$ dB, *dotted lines* denote $\sigma_\Omega = 4$ dB, and *dot-dashed lines* denote $\sigma_\Omega = 8$ dB

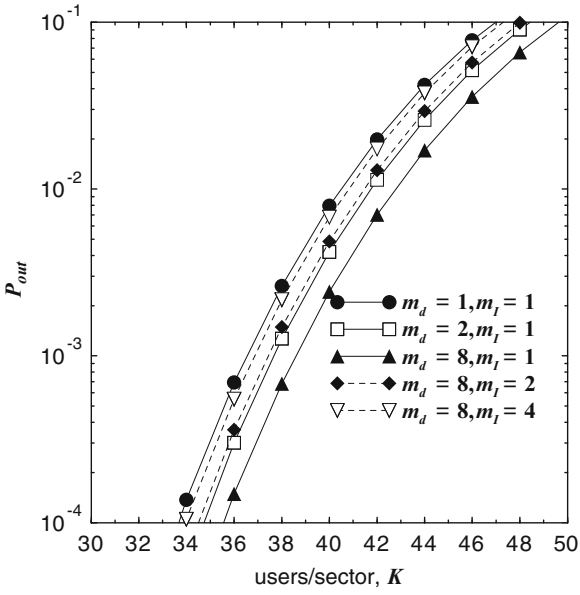

Fig. 12.4 Reverse channel capacity for different Nakagami shape factors with $\gamma_{b\ req} = 7$ dB, $\sigma_\Omega = 8$ dB

consider the first tier of interfering cells. Observe that the frequency reuse efficiency decreases with the shadow standard deviation, σ_Ω, and slightly increases when m_d increases or m_I decreases.

To show that the values of θ and f in Table 12.1 do not depend on the number of users per cell, K, we derive the cdf of the out-of-cell interference to the in-cell interference $I_\mathrm{o}/I_\mathrm{in}$ for the reverse channel as

Table 12.1 Ratio of the mean of out-of-cell interference to the mean in-cell interference, θ, and frequency reuse efficiency, f, under different propagation conditions

m_d	m_I	σ_Ω, dB	θ	$f = 1/(1+\theta)(\%)$
8	8	8	60.14%	62.45
8	4	8	58.83%	62.96
8	2	8	56.20%	64.02
8	1	8	51.11%	66.1i8
4	1	8	52.36%	65.63
2	1	8	54.90%	64.56
1	1	8	59.73%	62.61
1	1	10	57.34%	63.56
1	1	6	60.16%	62.44
1	1	4	57.82%	63.36
1	1	No shadowing	51.76%	65.89
No fading	No fading	No shadowing	21.81%	82.10
No fading	No fading	4	39.42%	71.73
No fading	No fading	8	60.02%	62.49
No fading	No fading	10	61.65%	61.86

$$\begin{aligned} \mathrm{P}[I_o/I_{in} < z] &= \mathrm{P}\left[\frac{I_o/C}{I_{in}/C} < z\right] \\ &= 1.0 - \mathrm{P}[I_o/C > z\, I_{in}/C] \\ &= 1.0 - \sum_{k=0}^{K-1} \binom{K-1}{k} \eta^k (1-\eta)^{K-1-k} Q\left(\frac{kz - \mathrm{E}[I_o/C]}{\sqrt{\mathrm{Var}[I_o/C]}}\right). \end{aligned} \quad (12.28)$$

Figure 12.5 plots the distribution of I_o/I_{in} (in dB) with different shadow standard deviations. Although the distribution varies with K, the mean value $\mathrm{E}[I_o/I_{in}]$ remains almost the same, that is, all the curves cross at the 50% point. This implies that the values of θ and f in Table 12.1 do not depend on K.

12.2.2 Forward Link Capacity

For the forward channel, a pilot signal is transmitted from each BS. The pilot signal causes interference in every cell, thereby reducing the capacity. However, this is offset by a decrease in $\gamma_{b\ req}$ due to coherent demodulation. With forward channel balancing power control, the mobile measures the received signal and periodically transmits the measurement to its serving BS [110]. When the total power requested by mobiles is below the maximum allowable transmit power, the BS will reduce its transmit power, thereby reducing interference; otherwise, the BS will redistribute the power from the forward links with good quality to those with poor quality.

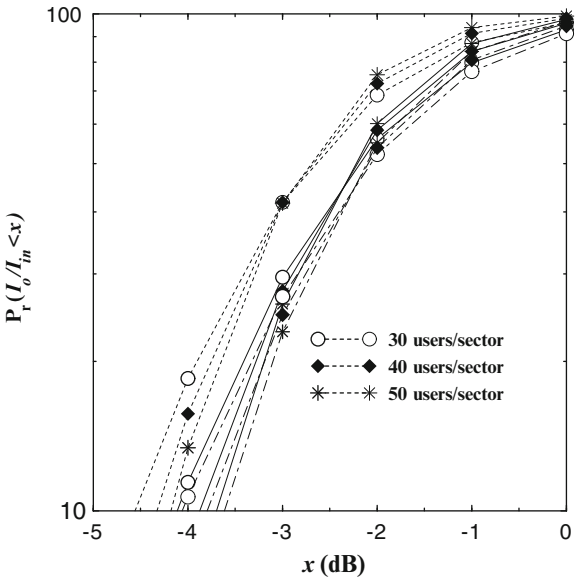

Fig. 12.5 Distribution of out-of-cell interference to in-cell interference, I_o/I_{in}, for the reverse channel. *Solid lines* denote $\sigma_\Omega = 0$ dB, *dotted lines* denote $\sigma_\Omega = 4$ dB, and *dot-dashed lines* denote $\sigma_\Omega = 8$ dB; $m_d = 1, m_l = 1$ (Rayleigh fading)

In the worst case situation, each BS always transmits with the maximum allowable power $P_{\max}$. From (12.24), the γ_b at the ith mobile under this condition is

$$\gamma_{b,i} = \frac{W_{ss}/W}{(I/C)_i} = \frac{W_{ss}/W}{(\sum_{j=0}^{M} C_{T_j} - \delta\phi_i C_{T_0})/\delta\phi_i C_{T_0}}, \tag{12.29}$$

$$C_{T_j} = P_{\max} 10^{\frac{\varsigma_j}{10}}, \tag{12.30}$$

where M is the number of surrounding BSs that are included in the calculation, C_{T_j} the received power from BS_j, $1-\delta$ the fraction of the total power allocated to the pilot, and the weighting factor ϕ_i is the fraction of the remaining power allocated to the ith mobile. Forward channel transmissions to MSs located in the shaded sectors of Fig. 12.6 will cause multiple-access interference with the forward channel transmission to the reference MS. As in [110] our results assume that 20% of the total BS transmit power is allocated to the pilot signal. Once again, the ς_i in decibel units are Gaussian random variables due to shadow and fading variations, with means and variances obtained from (2.314).

The BS distributes its transmit power proportionally according to the needs of each mobile within its cell. This is accomplished by first obtaining the required ϕ_i for each mobile, $(\phi_i)_{req}$, by setting $\gamma_b = \gamma_{b\,req}$ in (12.29). To account for the voice activity, we then calculate the modified weighting factor [145]

$$\overline{\phi_i} = \frac{(\phi_i)_{req}}{\sum_{\substack{j=1 \\ j\neq i}}^{K} \chi_j (\phi_j)_{req} + (\phi_i)_{req}}. \tag{12.31}$$

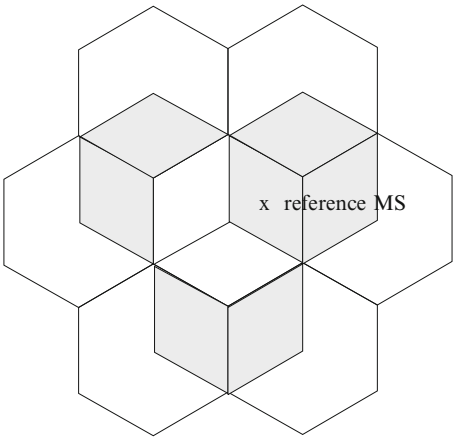

Fig. 12.6 Forward channel transmissions to MSs located in the *shaded areas* will cause multiple-access interference with the forward channel transmission to the reference MS

The power balancing scheme in [47] does the same thing, except that the voice activity factors, χ_j, are not considered. The outage probability then becomes

$$\begin{aligned} P_{\text{out}} &= \mathrm{P}\left[\gamma_{\text{b}} < \gamma_{\text{b req}}\right] \\ &= \mathrm{P}\left[\overline{\phi_i} < (\phi_i)_{\text{req}}\right]. \end{aligned} \tag{12.32}$$

Numerical results can be obtained from the last equation in (12.32) using Monte Carlo simulation techniques to account for the random user locations, and shadow and fading variations. For each set of MS locations and propagation conditions, we first determine the required fraction of power, $(\phi_i)_{\text{req}}$, needed to meet the $\gamma_{\text{b req}}$ requirement. Afterwards, we find if the actual power allocation for each MS, $\overline{\phi_i}$, is sufficient.

Figure 12.7 shows how the forward channel capacity depends on $\gamma_{\text{b req}}$ and the shadow standard deviation. Shadowing has a slightly stronger effect on forward channel capacity compared to the reverse channel. Figure 12.8 shows the forward channel capacity for various Nakagami shape factors. The Nakagami shape factor also plays a significant role in forward channel capacity, and overly optimistic capacity estimates will be obtained if fading is neglected.

12.2.3 Imperfect Power Control

Any power control algorithm will inevitably be subject to some degree of error. It has been experimentally verified that the power control error (in dB) can be modeled as a zero-mean Gaussian random variable with variance σ_{E}^2 [145, 194]. For the reverse channel, (12.10) has the modified form

$$C10^{\zeta_{\text{E}j}/10} = P_{i,j}10^{\zeta_d/10}, \tag{12.33}$$

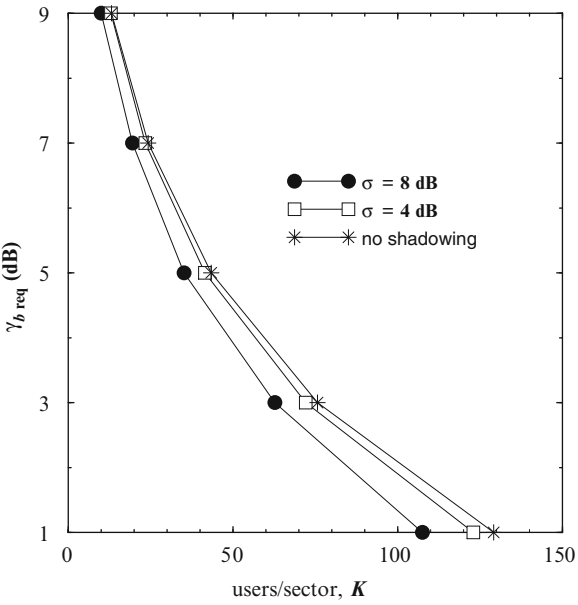

Fig. 12.7 Forward channel capacity with $P_{\text{out}} = 10^{-2}$ for different $\gamma_{\text{b req}}$; the Nakagami shape factors are $m_{\text{d}} = 1$ and $m_{\text{I}} = 1$ (Rayleigh fading), and σ_{Ω} is the shadow standard deviation

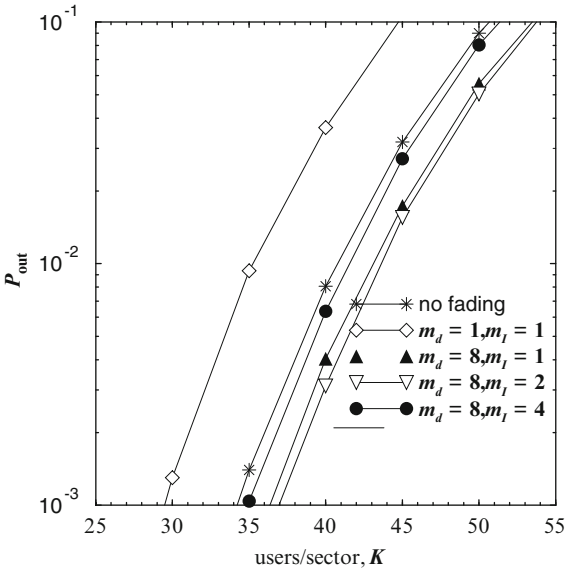

Fig. 12.8 Forward channel capacity for different Nakagami shape factors with $\gamma_{\text{b req}} = 5\,\text{dB}$, $\sigma_{\Omega} = 8\,\text{dB}$

where ς_{E_j} is the power control error. The mean and variance of $x = \varsigma_{i,0} - \varsigma_{i,j}$ with imperfect power control are similar to (12.18), but have the form

$$\mu_{x\ (\text{dB})} = \mu_{i,0\ (\text{dBm})} - \mu_{i,j\ (\text{dBm})}, \tag{12.34}$$

$$\sigma_x^2 = \sigma_{i,0}^2 + \sigma_{i,j}^2 + \sigma_{\text{E}}^2. \tag{12.35}$$

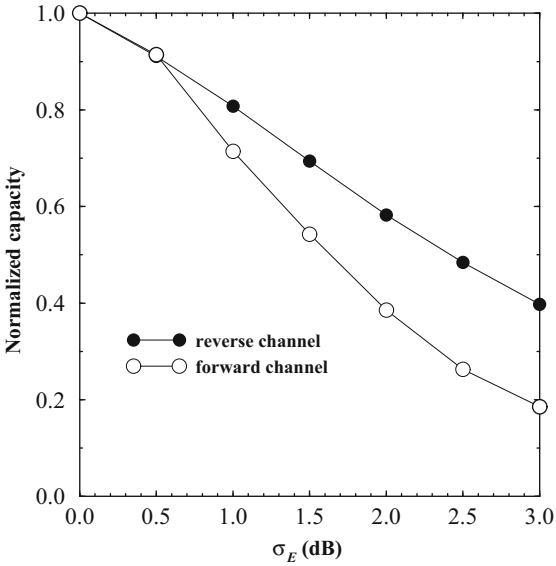

Fig. 12.9 Forward and reverse channel capacity with imperfect power control. The capacity is normalized with respect to the capacity with perfect power control; σ_{E} is the standard deviation of the power control error, $m_{\mathrm{d}} = 1$, $m_{\mathrm{I}} = 1$, and $\sigma_{\Omega} = 8$ dB

With imperfect power control, the in-cell interference experienced by $\mathrm{MS}_{0,i}$ at the reference BS, BS_0, is $I_{\mathrm{in}} = C\kappa$, where

$$\kappa = \sum_{\substack{j=1 \\ j \neq i}}^{K} 10^{\zeta_{\mathrm{E}j}/10} \chi_j. \tag{12.36}$$

Then

$$\begin{aligned} P_{\mathrm{out}} &= \mathrm{P}[\gamma_{\mathrm{b}} < \gamma_{\mathrm{b\ req}}] \\ &= \mathrm{P}[I_{\mathrm{o}}/C + I_{\mathrm{in}}/C > (I/C)_{\gamma_{\mathrm{b\ req}}}] \\ &= \mathrm{P}[I_{\mathrm{o}}/C > (I/C)_{\gamma_{\mathrm{b\ req}}} - \kappa] \\ &= \sum_{k=0}^{K-1} \binom{K-1}{k} p^k (1-p)^{K-1-k} \\ &\quad \times \int_0^{\infty} \mathrm{P}\left[I_{\mathrm{o}}/C > (I_{\mathrm{o}}/C)_{\gamma_{\mathrm{b\ req}}} - \kappa | \kappa \right] p(\kappa|k) d\kappa. \end{aligned} \tag{12.37}$$

Note that the conditional pdf of κ given k, $p(\kappa|k)$, is approximately log-normal. The log-normal approximation can be calculated using the Fenton–Wilkinson or Schwartz and Yeh methods discussed in Sect. 3.1. Observe from Fig. 12.9 that the reverse channel capacity is dramatically decreased as the power control error increases. For $P_{\mathrm{out}} = 0.01$ and power control errors of $\sigma_{\mathrm{E}} = 1$, 2, and 3 dB, the reverse channel capacity is decreased by 24%, 50%, and 68%, respectively.

To consider the effect of power control error on the forward channel, (12.31) becomes

$$\overline{\phi_i} = \frac{\phi_i 10^{\zeta_{\mathrm{E}_i}/10}}{\sum_{\substack{j=1 \\ j\neq i}}^{K} \chi_j \phi_j 10^{\zeta_{\mathrm{E}_j}/10} + \phi_i 10^{\zeta_{\mathrm{E}_i}/10}}. \tag{12.38}$$

Figure 12.9 shows that the forward channel capacity is reduced by 31%, 64%, and 83% for $\sigma_{\mathrm{E}} = 1.0$, 2.0, and 3.0 dB, respectively. Note that imperfect power control has a more severe effect on the forward channel than the reverse channel for the same propagation conditions.

12.3 Hierarchical Macrodiversity CDMA Cellular Architectures

CDMA cellular systems often use hierarchical architectures consisting of macrocells with underlaid microcells. In such architectures, macrocells cover large areas with sparse traffic densities, whereas microcells serve small areas with high traffic densities. However, due to their effective frequency reuse factor of 1, hierarchical CDMA systems must deal with cross interference between the hierarchical layers. This cross-layer interference can be subdued by assigning distinct spectrum to each layer, but this will make inefficient use of the available spectrum. A better approach allows the hierarchical layers to share the same spectrum.

For the reverse link, one possibility is hierarchical maximum ratio combining (HMRC), where the signal from each mobile station (MS) is received by several BSs in both hierarchical layers and coherently combined. If we assume independent interference at the different BS locations, the combined CIR is the algebraic sum of the CIRs at each BS

$$(C/I)_{\mathrm{HMRC}} = \sum_{i=1}^{N} (C/I)_{\mu,i} + \sum_{j=1}^{M} (C/I)_{\mathrm{M},j}, \tag{12.39}$$

where N and M are the number of BSs involved in the combining, and the subscripts μ and M designate "microcell" and "macrocell," respectively.

MMRC has been proven to be an effective way of improving the capacity in cellular CDMA systems [117, 127]. In [127], Hanly proved the existence of a power control solution using MMRC, and showed that the capacity is unaffected by outside interference. In [117], by assuming equal reverse interference level at each BS in non-hierarchical settings, Gorricho and Paradells constructed a simple proof showing that MMRC reverse link capacity is close to an isolated cell capacity. Here we generalize the results in [117] and apply them to hierarchical CDMA systems. We will derive an analytical solution for HMRC reverse performance without assuming an equal level of reverse link interference among cells, and show that both microcell and macrocell performances are nearly unaffected by each other's presence.

The reverse link is commonly considered to limit the CDMA system capacity. However, with the emergence of asymmetric wireless data services, the forward link performance has become increasingly important. For the forward link, HMRC-like combining schemes are not suitable because such schemes will increase the forward link interference [135]. One possible solution is selective transmit diversity (STD) where each BS provides multiple transmit paths by means of spatially separated antennas, and the system allows each MS to connect to the most robust path among the multiple paths [136, 168].

12.3.1 System Model

Consider a hierarchical CDMA deployment consisting of a group of omnidirectional macrocells and a cluster of omnidirectional microcells embedded within the macrocells. The MSs are assumed to be uniformly distributed in both macrocells and microcells, yet the load condition of each cell might differ. Although we do not assume any particular load conditions, microcells are generally more densely populated by MSs than macrocells. We note that with macrodiversity, there are no longer distinct boundaries between cells and hierarchical layers. Therefore, MSs are referenced to their respective locations. For example, a microcell MS means that the MS is physically located in the designated microcell area, but not necessarily served by it.

The radio links are assumed to be affected by Rayleigh fading and log-normal shadowing. The composite distribution of the link gain, G, is given by the Gamma-log-normal density in (2.313) with $m = 1$, that is,

$$f_G(x) = \int_0^\infty \frac{1}{\Omega_\mathrm{p}} \mathrm{e}^{-x/\Omega_\mathrm{p}} \frac{1}{\sqrt{2\pi}\xi\,\sigma_\Omega \Omega_\mathrm{p}} \exp\left\{ -\frac{\left(10\log_{10}\{\Omega_\mathrm{p}\} - \mu_{\Omega_{\mathrm{p}\ (\mathrm{dBm})}}\right)^2}{2\sigma_\Omega^2} \right\} \mathrm{d}\Omega_\mathrm{p}, \tag{12.40}$$

where σ_Ω is the shadow standard deviation, $\xi = \ln(10)/10$ and $\mu_{\Omega_{\mathrm{p}\ (\mathrm{dBm})}}$ is the area mean that depends on the path loss model. Here, we use the simple path loss model

$$\mu_{\Omega_{\mathrm{p}\ (\mathrm{dBm})}}(d) = \mu_{\Omega_{\mathrm{p}\ (\mathrm{dBm})}}(d_\mathrm{o}) - 10\beta \log_{10}\{d/d_\mathrm{o}\} \ \ (\mathrm{dBm}), \tag{12.41}$$

where $\mu_{\Omega_{\mathrm{p}\ (\mathrm{dBm})}}(d_\mathrm{o})$ is the area mean at a reference distance d_o, d the distance between the MS and BS, β the path loss exponent. As shown in (2.314), the composite Gamma-log-normal distribution in (12.40) can approximated by a log-normal distribution with parameters

$$\begin{aligned} \mu_{(\mathrm{dBm})} &= \mu_{\Omega_{\mathrm{p}\ (\mathrm{dBm})}} - 2.50675, \\ \sigma^2 &= \sigma_\Omega^2 + 31.0215. \end{aligned} \tag{12.42}$$

Fig. 12.10 Single cell model

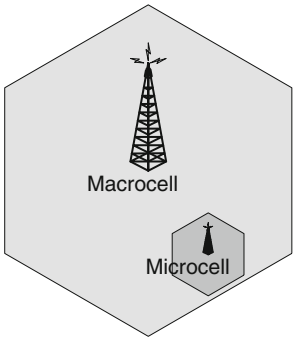

In other words, the link gain G in decibels, denoted by $\varsigma = 10\log_{10}\{G\}$ is normally distributed with the mean $\mu_{(\mathrm{dBm})}$ and variance σ^2 in (12.42).

12.3.2 Reverse Link Analysis

We first consider a simple single macrocell and microcell system to introduce the method of HMRC analysis. Then, we extend the analysis to a multicell system.

12.3.2.1 Single Cell Model

Consider a single microcell embedded within a macrocell as shown in Fig. 12.10. Using HMRC, the reverse link CIR of MS_i is

$$\begin{aligned}(C/I)_i &= (C/I)_{\mu,i} + (C/I)_{\mathrm{M},i} \\ &= \frac{C_{\mu,i}}{I_{\mu,i}} + \frac{C_{\mathrm{M},i}}{I_{\mathrm{M},i}},\end{aligned} \tag{12.43}$$

where $C_{\mu,i}$ and $C_{\mathrm{M},i}$ are the received signal power at the microcell BS and macrocell BS, respectively. Let $\lambda_i = I_{\mu,i}/I_{\mathrm{M},i}$ be the ratio of the microcell interference to macrocell interference. Then $(C/I)_i$ becomes

$$\begin{aligned}(C/I)_i &= \frac{C_{\mu,i} + \lambda_i C_{\mathrm{M},i}}{I_{\mu,i}} \\ &= \frac{(G_{\mu,i} + \lambda_i G_{\mathrm{M},i})P_i}{I_{\mu,i}} \\ &= \frac{C_{\mathrm{reverse},i}}{I_{\mu,i}},\end{aligned} \tag{12.44}$$

where $G_{\mu,i}$ and $G_{\mathrm{M},i}$ are the reverse link gains associated with the microcell BS and macrocell BS.

The HMRC reverse power control algorithm controls each MS transmit power, P_i, so that all MS experience a uniform CIR level. The convergence of such power control policy has been proven in [294]. Let us assume that the microcell BS and macrocell BS both serve a large number of MSs such that the microcell and macrocell interference levels experienced by each MS are nearly the same, that is,

$$I_{\mu,i} \approx I_{\mu}, \quad I_{M,i} \approx I_{M}\ , \ \forall\, i. \tag{12.45}$$

Since the interference power is the difference between the total received power and the desired signal power, the differences in the desired signal components have minimal effect on interference values when the system load is relatively large. This also suggests that the variation in λ_i is minimal. The above assumption is justified in the numerical results section that follows below. Based on the assumption in (12.45), HMRC power control now results in all MSs having the same uniform combined signal power, C_{reverse}.

Let N and M be the number of MSs located in the microcell and macrocell, respectively, and express $I_{\mu,i}$ and $I_{M,i}$ as follows:

$$\begin{aligned} I_{\mu,i} &= \sum_{j\neq i}^{N} C_{\mu,j}|_{\mu} + \sum_{k=1}^{M} C_{\mu,k}|_{M}, \\ I_{M,i} &= \sum_{j\neq i}^{N} C_{M,j}|_{\mu} + \sum_{k=1}^{M} C_{M,k}|_{M}\ , \quad i \in \text{microcell} \end{aligned} \tag{12.46}$$

and

$$\begin{aligned} I_{\mu,i} &= \sum_{j=1}^{N} C_{\mu,j}|_{\mu} + \sum_{k\neq i}^{M} C_{\mu,k}|_{M}, \\ I_{M,i} &= \sum_{j=1}^{N} C_{M,j}|_{\mu} + \sum_{k\neq i}^{M} C_{M,k}|_{M}\ , \quad i \in \text{macrocell}, \end{aligned} \tag{12.47}$$

where $C_{\text{BS}j,i}|_{\text{BS}k}$ is the received signal power at BSj from MS$_i$ given that MS$_i$ is located in the cell served by BSk, and BSj, BS$k \in \{\mu, M\}$. Let us first consider the case for the microcell MS. From (12.44) we can deduce that $C_{M,i} = (C_{\text{reverse}} - C_{\mu,i})/\lambda_i$. Therefore,

$$\begin{aligned} \lambda_i &= \frac{I_{\mu,i}}{I_{M,i}} \\ &= \frac{I_{\mu,i}}{\sum_{j\neq i}^{N} C_{M,j}|_{\mu} + \sum_{k=1}^{M} C_{M,k}|_{M}} \\ &= \frac{I_{\mu,i}}{\sum_{j\neq i}^{N} (C_{\text{reverse}} - C_{\mu,j}|_{\mu})/\lambda_j + \sum_{k=1}^{M} (C_{\text{reverse}} - C_{\mu,k}|_{M})/\lambda_k} \end{aligned}$$

$$\approx \frac{\lambda_i I_{\mu,i}}{\sum_{j\neq i}^{N}(C_{\text{reverse}} - C_{\mu,j|\mu}) + \sum_{k=1}^{M}(C_{\text{reverse}} - C_{\mu,k|\text{M}})},$$

$$= \frac{\lambda_i I_{\mu,i}}{(N+M-1)C_{\text{reverse}} - I_{\mu,i}}. \tag{12.48}$$

where the approximation in the second last line uses the fact that $\lambda_j \approx \lambda_k \ \forall \ j,k$. Solving the above equation for $I_{\mu,i}$ gives

$$I_{\mu,i} \approx \frac{(N+M-1)C_{\text{reverse}}}{2}. \tag{12.49}$$

Using the similar approach, one can see that the macrocell MS yields the same result. Then, the reverse link CIR can be approximated as follows:

$$(C/I)_i = \frac{C_{\text{reverse}}}{I_{\mu,i}} \approx \frac{2}{N+M-1}. \tag{12.50}$$

We make some important observations about HMRC from (12.50). First, the CIR performance is independent of the microcell location. Without HMRC, the overall performance suffers from increased level of inter-layer cross interference in cases where the microcell is closer to the macrocell BS. For HMRC, however, the combining effect is directly related to the proximity of the two BSs. Therefore, the increase in combining effect compensates for the increase in interference due to the microcell. Another noteworthy observation is that the HMRC performance is only limited by the overall system load, $N+M$, and not by individual cell loads. An overloaded microcell does not affect the system performance as long as the overall system load is kept under check, whereas it can dictate the system performance for non-HMRC systems. This suggests that HMRC is an effective way to share available resources between hierarchical layers.

12.3.2.2 Multiple Cell Model

We now extend the above analysis to multiple cell environments. Our multicell model consists of three macrocells and a cluster of K microcells embedded within the macrocells as shown in Fig. 12.11. Then,

$$\begin{aligned}(C/I)_i &= (C/I)_{\mu 1,i} + \cdots + (C/I)_{\mu K,i} + (C/I)_{\text{M1},i} + \cdots + (C/I)_{\text{M3},i} \\ &= \frac{C_{\mu 1,i} + \cdots + \lambda_{\mu K,i} C_{\mu K,i} + \lambda_{\text{M1},i} C_{\text{M1},i} + \cdots + \lambda_{\text{M3},i} C_{\text{M3},i}}{I_{\mu 1,i}} \\ &= \frac{C_{\text{reverse},i}}{I_{\mu 1,i}},\end{aligned} \tag{12.51}$$

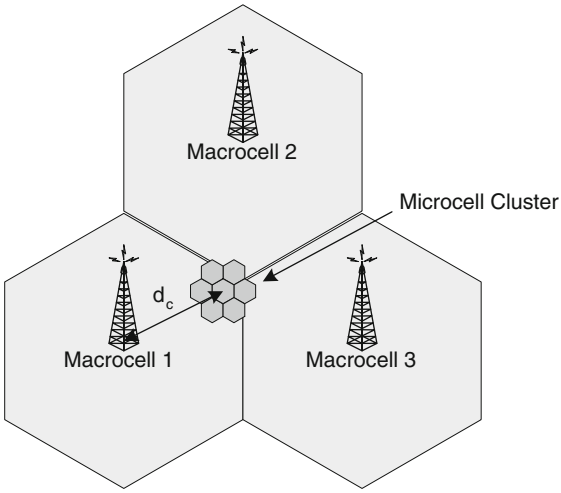

Fig. 12.11 Multiple cell model

where $\lambda_{\mathrm{BS}j,i} = I_{\mu 1,i}/I_{\mathrm{BS}j,i}$. Let N_i and M_j be the number of MSs in microcell i and macrocell j, respectively. Then, for the microcell 1 MSs,

$$\begin{aligned} I_{\mathrm{M1},i} &= \sum_{j\neq i}^{N_1} C_{\mathrm{M1},j}|_{\mu 1} + \cdots + \sum_{l=1}^{N_K} C_{\mathrm{M1},l}|_{\mu K} + \sum_{p=1}^{M_1} C_{\mathrm{M1},p}|_{\mathrm{M1}} + \cdots + \sum_{r=1}^{M_3} C_{\mathrm{M1},r}|_{\mathrm{M3}} \\ &\approx (N_1 + \cdots + N_K + M_1 + M_2 + M_3 - 1)\frac{C_{\mathrm{reverse}}}{\lambda_{\mathrm{M1},i}} - (2+K)\frac{I_{\mu 1,i}}{\lambda_{\mathrm{M1},i}}. \end{aligned} \tag{12.52}$$

Therefore,

$$\begin{aligned} I_{\mu 1,i} &\approx \frac{(N_1 + \cdots + N_K + M_1 + M_2 + M_3 - 1)C_{\mathrm{reverse}}}{3+K}, \\ (C/I)_i &\approx \frac{3+K}{N_1 + \cdots + N_K + M_1 + M_2 + M_3 - 1}. \end{aligned} \tag{12.53}$$

Using MSs in other cells with their corresponding values of λ will yield the same result. We can make the same important observations we made in the single cell case for the multicell case also. Note also that if both microcells and macrocells are loaded with an equal number of MSs, the result in (12.53) is the same as the result obtained in [117]. This tells us that the macrocell capacity is nearly unaffected by the introduction of microcells when inter-layer HMRC is allowed.

12.3.2.3 Numerical Results

Consider the deployment in Fig. 12.10 where the radii of the macrocell and microcell regions are 1,500 m and 200 m, respectively. The propagation environment

Table 12.2 Single cell model result

N	M	$\text{CIR}_{\text{anal.}}$ dB	$\text{CIR}_{\text{sim.}}$ dB
10	10	−9.60	−9.78
15	10	−10.66	−10.79
20	15	−12.21	−12.30
20	20	−12.82	−12.90

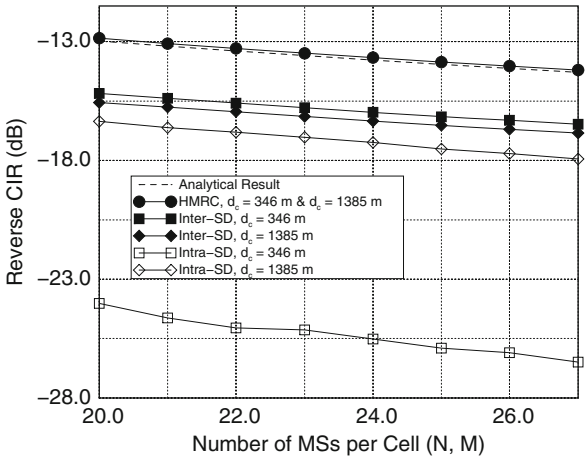

Fig. 12.12 Reverse link CIR performance comparison

is characterized by a path loss exponent of 4 and a shadow standard deviation of 8 dB. Table 12.2 shows the average performance comparison between analytical and simulation results obtained using the single cell model. Small deviations between the analytical and simulation results are most likely caused by the equal interference assumption in (12.45) while deriving the analytical solution. The fact is that MSs located close to a BS will experience less interference, while MSs further away from the BS will face higher interference. However, the difference is marginal and it becomes smaller as the system load increases.

Figure 12.12 shows the multicell reverse link CIR performance comparison between HMRC and non-HMRC diversity power control schemes at various microcell cluster locations (d_c). A three-macrocell and three-microcell model is used to obtain the simulation results. Both macrocells and microcells are loaded with the same number of MSs. Two non-HMRC diversity schemes are compared; intra-layer selection diversity (intra-SD) and inter-layer selection diversity (inter-SD). With intra-SD the most robust link within each layer is selected, while inter-SD allows each MS to connect the best BS in any layer. Clearly, HMRC performance is superior to that of non-HMRC schemes. It is observed that both macrocell and microcell capacities are nearly unaffected by each other's presence (i.e., both macrocells and microcells retain a near isolated cell capacity). The performances of both SD schemes are dependent of the microcell cluster location, d_c. For intra-SD, the cross interference between the layers increases as the microcell cluster gets closer to a macrocell BS, and causes overall system performance degradation.

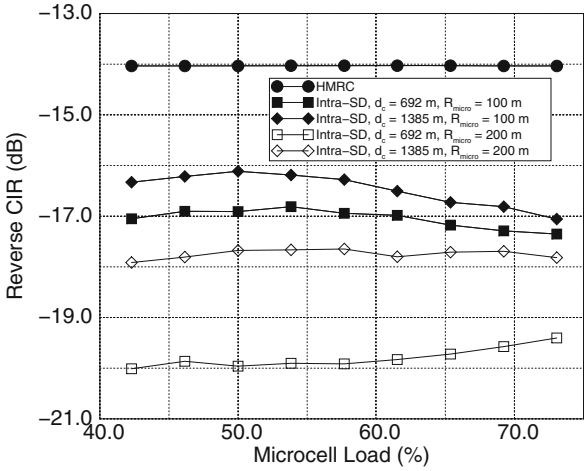

Fig. 12.13 Intra-SD CIR performance against microcell load

For inter-SD, the diversity gain decreases as d_c increases, which also causes the performance to suffer. However, using HMRC eliminates the effect of the cluster location on the CIR performance. From (12.51) one can see that the reverse CIR performance of HMRC is proportional to the λ_i and macrocell gains. These two factors balance the performance as the microcell cluster location changes. When d_c is small, the cross interference causes the λ_i to decrease, but the loss is compensated by the increase in macrocell gains. Conversely, when d_c is large the macrocell gains decrease while the λ_i increase.

The analytical results indicate that the HMRC performance is a function of the overall system load, and does not depend on either the load distribution between the layers, or the cell sizes. Figures 12.13 and 12.14 show the effect of microcell load and size on the reverse link CIR performance. The same three-multicell model is used in this simulation also. The overall system load is kept at 156 MSs while the microcell load percentage to the overall load is varied. It is observed that in nearly all instances both non-HMRC schemes suffer performance losses with an increase in the microcell load percentage and microcell radius, R_{micro}. It can be understood that the increase in the overall interference due to an increased microcell load cannot be relieved entirely by a decreased macrocell load. Larger microcell sizes also increase interference, since MSs belong to microcells need to transmit at higher power levels. The performance of HMRC is not affected by the microcell load and size changes, as predicted. The increase in microcell interference also increases the λ_i, which offsets the negative effect of the microcell interference. Therefore, HMRC allows flexible resource sharing between hierarchical layers.

Our observations suggest that implementing HMRC gives system planners and administrators almost unlimited freedom and flexibility when contemplating microcell placements. With HMRC, microcell(s) can be placed anywhere within the existing macrocell layer, significant performance and capacity gains can be obtained while guaranteeing robust resource sharing between the layers.

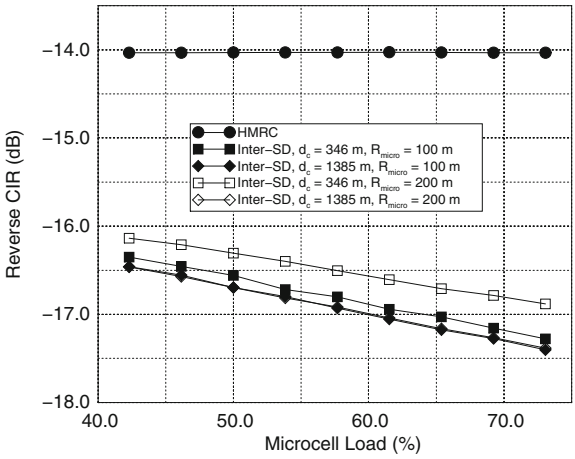

Fig. 12.14 Inter-SD CIR performance against microcell load

12.3.3 Forward Link Analysis

The forward power control scheme considered here is based on the neighboring-cell pilot power (NPP) scheme proposed in [135], where the forward transmit power to each MS is determined according to link conditions between the MS and surrounding BSs. To see how the NPP scheme can be applied to a hierarchical CDMA architecture, consider a deployment of K microcells surrounded by three macrocells as in Fig. 12.11. Let $P^t_{\mathrm{M}j}$ and $P^t_{\mu k}$ be the total powers transmitted by the BSs serving macrocell j and microcell k, respectively. Then, the interference experienced by MS_i can be estimated as

$$I_i \approx G_{\mathrm{M1},i}P^t_{\mathrm{M1}} + \cdots + G_{\mathrm{M3},i}P^t_{\mathrm{M3}} + G_{\mu 1,i}P^t_{\mu 1} + \cdots + G_{\mu K,i}P^t_{\mu K}. \tag{12.54}$$

Define the power ratio $\gamma_{\mathrm{BS}j} = P^t_{\mu 1}/P^t_{\mathrm{BS}j}$. Only one BS can transmit to MS_i at any given time and the transmit power is determined by

$$P_{\mathrm{BS}j,i} = \frac{\frac{1}{\gamma_{\mathrm{M1}}}G_{\mathrm{M1},i} + \cdots + \frac{1}{\gamma_{\mathrm{M3}}}G_{\mathrm{M3},i} + G_{\mu 1,i} + \cdots + \frac{1}{\gamma_{\mu K}}G_{\mu K,i}}{G_{\mathrm{BS}j,i}}P_{\mathrm{T}}, \tag{12.55}$$

when MS_i is connected to BS j and P_{T} is the predetermined forward transmit power constant. The resulting forward CIR for MS_i is then

$$\begin{aligned}(C/I)_i &= \frac{C_i}{I_i} \\ &\approx \frac{(\frac{1}{\gamma_{\mathrm{M1}}}G_{\mathrm{M1},i} + \cdots + \frac{1}{\gamma_{\mathrm{M3}}}G_{\mathrm{M3},i} + G_{\mu 1,i} + \cdots + \frac{1}{\gamma_{\mu K}}G_{\mu K,i})P_{\mathrm{T}}}{(\frac{1}{\gamma_{\mathrm{M1}}}G_{\mathrm{M1},i} + \cdots + \frac{1}{\gamma_{\mathrm{M3}}}G_{\mathrm{M3},i} + G_{\mu 1,i} + \cdots + \frac{1}{\gamma_{\mu K}}G_{\mu K,i})P^t_{\mu 1}} \\ &\approx \frac{P_{\mathrm{T}}}{P^t_{\mu 1}}.\end{aligned} \tag{12.56}$$

Notice that with NPP, every MS experiences the same forward CIR regardless of its location. While NPP does not offer any significant performance gain over conventional power control schemes, it does guarantee that every MS experiences the same forward link CIR.

The forward analysis consists of two parts; non-STD and STD cases. For non-STD case, there is no transmit diversity; each BS has only one antenna and provides single forward transmit path. Each MS connects to the BS which provides the most robust path. We use a single cell hierarchical model as in Fig. 12.10 for the forward analysis, since the concept can be readily extended to multicell environments. For the single macrocell/microcell model,

$$P_{\mathrm{BS}j,i} = \frac{G_{\mu,i} + (1/\gamma)G_{\mathrm{M},i}}{G_{\mathrm{BS}j,i}} P_{\mathrm{T}}, \tag{12.57}$$

where $\gamma = P_{\mu 1}^{\mathrm{t}}/P_{\mathrm{M}}^{\mathrm{t}}$ is the ratio between the microcell and macrocell total forward transmit powers, and $\mathrm{BS}j \in \{\mu, M\}$.

12.3.3.1 Nonselective Transmit Diversity

From the model in Sect. 12.3.1, the gain $G_{\mathrm{BS}j,i}$ has a composite Gamma-log-normal distribution that can be approximated by a purely log-normal distributed with the parameters given in (12.42). The mean $\mu_{(\mathrm{dBm})}$ in (12.42) depends on the distance between base station $\mathrm{BS}j$ and MS_i according to the path loss model in (12.41). This distance can be expressed as a function of the polar coordinates (r, θ) of the MS location referenced to $\mathrm{BS}j$, that is, $d_{\mathrm{BS}j}(r, \theta)$. Hence, we can write $G_{\mathrm{BS}j,i} = 10^{\varsigma_{\mathrm{BS}j}(r,\theta)/10}$, where $\varsigma_{\mathrm{BS}j}(r, \theta)$ is a normal random variable with mean $\mu_{(\mathrm{dBm})}$ and σ^2 in (12.42).

Suppose that the location of MS_i, (r, θ), is referenced with respect to the BS it is connected to. Then, the forward transmit power according to NPP is

$$\begin{aligned}
P_{\mu,i}(r,\theta) &= \frac{(1/\gamma)G_{\mathrm{M},i} + G_{\mu,i}}{G_{\mu,i}} P_{\mathrm{T}} \\
&= \left(\frac{G_{\mathrm{M},i}}{\gamma G_{\mu,i}} + 1\right) P_{\mathrm{T}} \\
&= \left(\frac{1}{\gamma} 10^{(\varsigma_{\mathrm{M}}(r,\theta) - \varsigma_{\mu}(r,\theta))/10} + 1\right) P_{\mathrm{T}} \\
&= \left(\frac{1}{\gamma} 10^{x(r,\theta)/10} + 1\right) P_{\mathrm{T}}, \quad \text{if } G_{\mu,i} > G_{\mathrm{M},i}, \\
P_{\mathrm{M},j}(r,\theta) &= \frac{(1/\gamma)G_{\mathrm{M},j} + G_{\mu,j}}{G_{\mathrm{M},j}} P_{\mathrm{T}} \\
&= \left(\frac{1}{\gamma} + \frac{G_{\mu,j}}{G_{\mathrm{M},j}}\right) P_{\mathrm{T}}
\end{aligned}$$

$$= \left(\frac{1}{\gamma} + 10^{(\varsigma_\mu(r,\theta)-\varsigma_M(r,\theta))/10}\right) P_T$$
$$= \left(\frac{1}{\gamma} + 10^{y(r,\theta)/10}\right) P_T\ ,\ \text{ if } G_{\mu,j} < G_{M,j}, \tag{12.58}$$

where $x(r,\theta) = \varsigma_M(r,\theta) - \varsigma_\mu(r,\theta)$, $y(r,\theta) = \varsigma_\mu(r,\theta) - \varsigma_M(r,\theta)$, and P_T is the forward transmit power constant. Let us now compute the conditional cumulative distribution functions (cdfs) of $Z = 10^{x(r,\theta)/10}$ and $W = 10^{y(r,\theta)/10}$ for the deployment shown in Fig. 12.10. First note that a microcell MS is physically located in the microcell area but may be served by either the microcell or macrocell BS. Also, a macrocell MS can be physically located anywhere in the macrocell area including the microcell area, and may be served by either the microcell or macrocell BS. It follows that:

$$F_Z(z|r,\theta) = \frac{P[10^{x(r,\theta)/10} < z|r,\theta]}{P[10^{x(r,\theta)/10} < 1|r,\theta]} = \frac{P[x(r,\theta) < 10\log_{10}(z)|r,\theta]}{P[x(r,\theta) < 0|r,\theta]}$$
$$= \Phi\left(\frac{10\log_{10}\{z\} - \mu_x(r,\theta)}{\sigma_x}\right)\left(\Phi\left(\frac{-\mu_x(r,\theta)}{\sigma_x}\right)\right)^{-1},\ 0 < z < 1, \tag{12.59}$$

$$F_W(w|r,\theta) = \Phi\left(\frac{10\log_{10}\{w\} - \mu_y(r,\theta)}{\sigma_y}\right)\left(\Phi\left(\frac{-\mu_y(r,\theta)}{\sigma_y}\right)\right)^{-1},\ 0 < w < 1, \tag{12.60}$$

where

$$\begin{aligned}
\mu_x(r,\theta) &= \mu_{\varsigma_M}(r,\theta) - \mu_{\varsigma_\mu}(r,\theta) \\
&= -\beta 10\log_{10}\{d_M(r,\theta)\} + \beta 10\log_{10}\{d_\mu(r,\theta)\}, \\
\mu_y(r,\theta) &= \mu_{\varsigma_\mu}(r,\theta) - \mu_{\varsigma_M}(r,\theta) \\
&= -\beta 10\log_{10}\{d_\mu(r,\theta)\} + \beta 10\log_{10}\{d_M(r,\theta)\}, \\
\sigma_x^2 &= \sigma_y^2 = 2(\sigma_\Omega^2 + 31.0254).
\end{aligned} \tag{12.61}$$

Then the cdfs of Z and W are

$$F_Z(z) = \begin{cases} \displaystyle\int_0^{2\pi}\int_0^{R_\mu} \frac{r}{\pi R_\mu^2} F_Z(z|r,\theta)\mathrm{d}r\mathrm{d}\theta\ , & \text{if MS} \in \text{microcell}, \\ \displaystyle\int_0^{2\pi}\int_0^{R_M} \frac{r}{\pi R_M^2} F_Z(z|r,\theta)\mathrm{d}r\mathrm{d}\theta\ , & \text{if MS} \in \text{macrocell}, \end{cases} \tag{12.62}$$

$$F_W(w) = \begin{cases} \displaystyle\int_0^{2\pi}\int_0^{R_{\mathrm{M}}} \frac{r}{\pi R_{\mathrm{M}}^2} F_W(w|r,\theta)\mathrm{d}r\mathrm{d}\theta\ , & \text{if MS} \in \text{macrocell}, \\ \displaystyle\int_0^{2\pi}\int_0^{R_\mu} \frac{r}{\pi R_\mu^2} F_W(w|r,\theta)\mathrm{d}r\mathrm{d}\theta\ , & \text{if MS} \in \text{microcell}. \end{cases} \tag{12.63}$$

Since both Z and W are nonnegative random variables, their expected values are as follows:

$$\begin{aligned} \mathrm{E}[Z] &= \int_0^{\infty} (1 - F_Z(z))\mathrm{d}z = \int_0^1 (1 - F_Z(z))\mathrm{d}z, \\ \mathrm{E}[W] &= \int_0^1 (1 - F_W(w))\mathrm{d}w. \end{aligned} \tag{12.64}$$

Let N and M be the number of MSs physically located in microcell and macrocell, respectively. Assuming there are N' microcell MS connected to microcell and M' macrocell MSs connected to macrocell, the expected value of the total forward transmit power by each BS is

$$\begin{aligned} \mathrm{E}[P_\mu|N',M'] &= N'P_{\mathrm{T}}\left(\frac{\mathrm{E}[Z|\text{MS} \in \text{microcell}]}{\gamma} + 1\right) \\ &\quad + (M - M')P_{\mathrm{T}}\left(\frac{\mathrm{E}[Z|\text{MS} \in \text{macrocell}]}{\gamma} + 1\right), \\ \mathrm{E}[P_{\mathrm{M}}|N',M'] &= (N - N')P_{\mathrm{T}}\left(\frac{1}{\gamma} + \mathrm{E}[W|\text{MS} \in \text{microcell}]\right) \\ &\quad + M'P_{\mathrm{T}}\left(\frac{1}{\gamma} + \mathrm{E}[W|\text{MS} \in \text{macrocell}]\right). \end{aligned} \tag{12.65}$$

We know that N' and M' are (N, Pr_μ) and $(M, \mathrm{Pr}_{\mathrm{M}})$ binomial random variables, respectively, where Pr_μ and Pr_{M} are the probabilities that an MS located in microcell and macrocell will connect to microcell and macrocell, respectively. Then,

$$\begin{aligned} \mathrm{E}[P_\mu] &= \sum_{N'=0}^{N} \binom{N}{N'} \mathrm{Pr}_\mu^{N'} (1 - \mathrm{Pr}_\mu)^{N-N'} \\ &\quad \times \sum_{M'=0}^{M} \binom{M}{M'} \mathrm{Pr}_{\mathrm{M}}^{M'} (1 - \mathrm{Pr}_{\mathrm{M}})^{M-M'} \mathrm{E}[P_\mu|N',M'], \\ \mathrm{E}[P_{\mathrm{M}}] &= \sum_{N'=0}^{N} \binom{N}{N'} \mathrm{Pr}_\mu^{N'} (1 - \mathrm{Pr}_\mu)^{N-N'} \\ &\quad \times \sum_{M'=0}^{M} \binom{M}{M'} \mathrm{Pr}_{\mathrm{M}}^{M'} (1 - \mathrm{Pr}_{\mathrm{M}})^{M-M'} \mathrm{E}[P_{\mathrm{M}}|N',M'], \end{aligned} \tag{12.66}$$

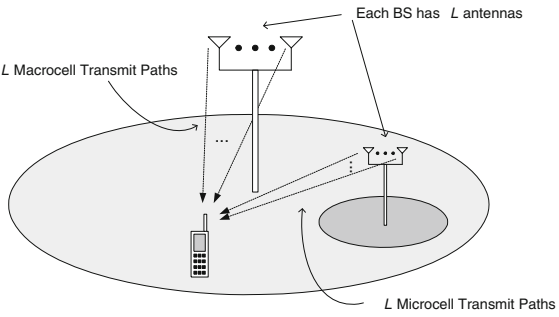

Fig. 12.15 Selective transmit diversity

where

$$\begin{aligned}\mathrm{Pr}_{\mu} &= \mathrm{P}\left[\mathrm{G}_{\mu,i} > \mathrm{G}_{\mathrm{M},i} | i \in \text{microcell}\right] \\ &= 1 - \int_0^{2\pi} \int_0^{R_{\mu}} \frac{r}{\pi R_{\mu}^2} \Phi\left(\frac{\mu_{\mathrm{M}}(r,\theta) - \mu_{\mu}(r,\theta)}{\sqrt{2(\sigma_{\Omega}^2 + 31.0254)}}\right) \mathrm{d}r\mathrm{d}\theta, \end{aligned} \tag{12.67}$$

$$\begin{aligned}\mathrm{Pr}_{\mathrm{M}} &= \mathrm{P}\left[\mathrm{G}_{\mathrm{M},j} > \mathrm{G}_{\mu,j} | j \in \text{macrocell}\right] \\ &= \int_0^{2\pi} \int_0^{R_M} \frac{r}{\pi R_M^2} \Phi\left(\frac{\mu_{\mathrm{M}}(r,\theta) - \mu_{\mu}(r,\theta)}{\sqrt{2(\sigma_{\Omega}^2 + 31.0254)}}\right) \mathrm{d}r\mathrm{d}\theta. \end{aligned} \tag{12.68}$$

We let $\gamma = \mathrm{E}[P_{\mu}]/\mathrm{E}[P_{\mathrm{M}}]$ and iterate until γ converges. Then the forward CIR is

$$\mathrm{CIR}_{\mathrm{non-STD}} = \frac{P_{\mathrm{T}}}{P_{\mu}} \approx \frac{P_{\mathrm{T}}}{\mathrm{E}[P_{\mu}]}. \tag{12.69}$$

12.3.3.2 Selective Transmit Diversity

In STD, each BS has a number of spatially separated antennas and an orthogonal pilot signal is transmitted from each antenna as shown in Fig. 12.15. In order for the fading conditions associated with different antennas to be sufficiently decorrelated (less than 0.7 correlation), the BS antenna separation needs to be on the order of ten wavelengths as shown in Sect. 2.1.6.1. By way of monitoring the pilot signals, an MS can select (mobile-assisted) the BS antenna that provides the most robust forward link until a better BS antenna is found. Therefore, only one BS antenna is selected to transmit at a time with STD, but the selected BS antenna will provide the best link among the multiple BS antennas. The main difference between STD and non-STD schemes is that STD provides multiple potential forward links per BS each with uncorrelated fading, while non-STD provides one forward link per BS. However, both STD and non-STD uses only one BS antenna to transmit at

a time. Diversity gain through antenna separation is viable at BS sites where the space and system complexity are less of limiting factors. We assume the antennas are separated sufficiently far apart that all potential forward links from the same BS have uncorrelated fading, but correlated shadowing.

Let us now assume that the microcell BS and macrocell BS each have L antennas, which means that the MS selects the best antenna out of a total of $2L$ antennas. Let $P_{\mathrm{BS}j}^{(l)}$ be the total forward transmit power by the lth transmit branch of BSj, where BS$j \in \{\mu, M\}$. Since the MSs are uniformly distributed, each transmit branch within a cell has an equal probability of being selected by the MSs and, therefore, we can assume that

$$\begin{aligned} P_{\mu}^{(i)} &\approx P_{\mu}^{(j)} \approx P_{\mu}^{\mathrm{STD}}, \\ P_{\mathrm{M}}^{(i)} &\approx P_{\mathrm{M}}^{(j)} \approx P_{\mathrm{M}}^{\mathrm{STD}}, \quad i \neq j. \end{aligned} \tag{12.70}$$

Then, the forward transmit power for MS$_i$ located at (r, θ) is

$$\begin{aligned} P_{\mu,i}^{\mathrm{STD}}(r,\theta) &= \frac{(1/\gamma_{\mathrm{STD}})(G_{\mathrm{M},i}^{(1)} + \cdots + G_{\mathrm{M},i}^{(L)}) + G_{\mu,i}^{(1)} + \cdots + G_{\mu,i}^{(L)}}{\max[G_{\mu,i}^{(1)}, \cdots, G_{\mu,i}^{(L)}]} P_{\mathrm{T}} \\ &\quad \text{if } \max[G_{\mu,i}^{(1)}, \cdots, G_{\mu,i}^{(L)}] > \max[G_{\mathrm{M},i}^{(1)}, \cdots, G_{\mathrm{M},i}^{(L)}]. \\ P_{\mathrm{M},i}^{\mathrm{STD}}(r,\theta) &= \frac{(1/\gamma_{\mathrm{STD}})(G_{\mathrm{M},i}^{(1)} + \cdots + G_{\mathrm{M},i}^{(L)}) + G_{\mu,i}^{(1)} + \cdots + G_{\mu,i}^{(L)}}{\max[G_{\mathrm{M},i}^{(1)}, \cdots, G_{\mathrm{M},i}^{(L)}]} P_{\mathrm{T}} \\ &\quad \text{if } \max[G_{\mu,i}^{(1)}, \cdots, G_{\mu,i}^{(L)}] < \max[G_{\mathrm{M},i}^{(1)}, \cdots, G_{\mathrm{M},i}^{(L)}], \end{aligned} \tag{12.71}$$

where $\gamma_{\mathrm{STD}} = P_{\mu}^{\mathrm{STD}}/P_{\mathrm{M}}^{\mathrm{STD}}$ and $G_{\mathrm{BS}j,i}^{(l)}$ is the gain associated with lth transmit branch of BSj to MS$_i$. Let $G_{\mathrm{BS}j,i} = \max[G_{\mathrm{BS}j,i}^{(1)}, \cdots, G_{\mathrm{BS}j,i}^{(L)}]$, then the cdf of $G_{\mathrm{BS}j,i}^{(l)}/G_{\mathrm{BS}j,i}$ is

$$\mathrm{P}[G_{\mathrm{BS}j,i}^{(l)}/G_{\mathrm{BS}j,i} < x] = \frac{\mathrm{P}[G_{\mathrm{BS}j,i}^{(l)}/G_{\mathrm{BS}j,i} < x]}{\mathrm{P}[G_{\mathrm{BS}j,i}^{(l)}/G_{\mathrm{BS}j,i} < 1]} \approx \frac{2x}{x+1}, \quad 0 < x < 1, \tag{12.72}$$

where $\mathrm{P}[G_{\mathrm{BS}j,i}^{(l)}/G_{\mathrm{BS}j,i} < x] = x/(x+1)$. The above result is accurate for $L = 2$ and adequate for $L = 3$ since the greatest diversity gain occurs between $L = 1$ and $L = 2$ as shown in Chap. 6. For two different cell locations, we can assume $G_{\mathrm{BS}k,i}^{(l)}$ and $G_{\mathrm{BS}j,i}$ are independent. Because the transmit paths from the same BS experience independent Rayleigh fading and the same shadowing, the conditional pdf and pdf of $G_{\mathrm{BS}j,i}$ are, respectively,

$$f_{G_{\mathrm{BS}j,i}}(x|\Omega_{\mathrm{p}}) = \frac{L}{\Omega_{\mathrm{p}}} \mathrm{e}^{-x/\Omega_{\mathrm{p}}} (1 - \mathrm{e}^{-x/\Omega_{\mathrm{p}}})^{L-1} \tag{12.73}$$

and

$$f_{G_{\mathrm{BS}j,i}}(x) = \int_0^\infty f_{G_{\mathrm{BS}j,i}}(x|\Omega_\mathrm{p})\frac{1}{\sqrt{2\pi}\xi\,\sigma_\Omega\Omega_\mathrm{p}} \times\exp\left\{-\frac{\left(10\log_{10}\{\Omega_\mathrm{p}\}-\mu_{\Omega_{\mathrm{p\ (dBm)}}}\right)^2}{2\sigma_\Omega^2}\right\}\mathrm{d}\Omega_\mathrm{p}. \quad (12.74)$$

It is shown in Appendix 1 that $f_{G_{\mathrm{BS}j,i}}(x)$ can be approximated by a purely log-normal distribution for $L=2$ with mean and variance given by

$$\begin{aligned}\mu_\mathrm{G} &= \xi^{-1}(\ln 2 - C) + \mu_\Omega = 0.503552 - \beta\log_{10}\{d\},\\ \sigma_\mathrm{G}^2 &= \xi^{-2}(\zeta(2,1) - 2(\ln 2)^2) + \sigma_\Omega^2 = 12.9016 + \sigma_\Omega^2,\end{aligned} \quad (12.75)$$

where $C \simeq 0.5772$ is Euler's constant and $\zeta(2,1) = \sum_{k=0}^{\infty} 1/(1+k)^2$ is Reimann's zeta function. Appendix 2 derives a similar approximation for $L=3$ where we obtain the following mean and variance:

$$\begin{aligned}\mu_\mathrm{G} &= \xi^{-1}(3\ln 2 - \ln 3 - C) + \mu_\Omega = 1.75294 - \beta\log_{10}\{d\},\\ \sigma_\mathrm{G}^2 &= \xi^{-2}(\zeta(2,1) - 12(\ln 2)^2 + 6(\ln 2)(\ln 3)) + \sigma_\Omega^2 = 8.4592 + \sigma_\Omega^2.\end{aligned} \quad (12.76)$$

Then the conditional cdf and cdf of $G_{\mathrm{BS}k,i}^{(l)}/G_{\mathrm{BS}j,i}$ are

$$\begin{aligned}\mathrm{P}[G_{\mathrm{BS}k,i}^{(l)}/G_{\mathrm{BS}j,i} < x|r,\theta] &= \frac{\mathrm{P}[G_{\mathrm{BS}k,i}^{(l)}/G_{\mathrm{BS}j,i} < x|r,\theta]}{\mathrm{P}[G_{\mathrm{BS}k,i}^{(l)}/G_{\mathrm{BS}j,i} < 1|r,\theta]}\\ &= \Phi\left(\frac{10\log_{10}(x) - \mu_{kj}(r,\theta)}{\sigma_{kj}}\right)\left(\Phi\left(\frac{-\mu_{kj}(r,\theta)}{\sigma_{kj}}\right)\right)^{-1}.\end{aligned} \quad (12.77)$$

$$\mathrm{P}[G_{\mathrm{BS}k,i}^{(l)}/G_{\mathrm{BS}j,i} < x] = \int_0^{2\pi}\int_0^{R_{\mathrm{BS}j}} \frac{r}{\pi R_{\mathrm{BS}j}^2}\mathrm{P}[G_{\mathrm{BS}k,i}^{(l)}/G_{\mathrm{BS}j,i} < x|r,\theta]\mathrm{d}r\mathrm{d}\theta, \quad 0 < x < 1, \quad (12.78)$$

where

$$\begin{aligned}\mu_{kj}(r,\theta) &= \mu_{\varsigma_{\mathrm{BS}k}}(r,\theta) - \mu_{\mathrm{G}_{\mathrm{BS}j}}(r,\theta)\\ &= -\beta 10\log_{10}\{d_{\mathrm{BS}k}(r,\theta)\} - 2.50675 + \mu_{\mathrm{G}_{\mathrm{BS}j}}(r,\theta),\\ \sigma_{kj}^2 &= \sigma_{\mathrm{BS}k}^2 + \sigma_\mathrm{G}^2\\ &= \sigma_\Omega^2 + 31.0254 + \sigma_\mathrm{G}^2.\end{aligned} \quad (12.79)$$

We can derive the expected values of $P_{\mu,i}^{\text{STD}}$ and $P_{\text{M},i}^{\text{STD}}$ using the same approach used in the previous section and get

$$\begin{aligned}
\text{E}[P_{\mu,i}^{\text{STD}}] &= \left(\frac{L}{\gamma_{\text{STD}}}\text{E}[Z] + (L-1)\text{E}[X] + 1\right) P_{\text{T}}, \\
\text{E}[P_{\text{M},i}^{\text{STD}}] &= \left(\frac{L-1}{\gamma_{\text{STD}}}\text{E}[Y] + L\text{E}[W] + \frac{1}{\gamma_{\text{STD}}}\right) P_{\text{T}},
\end{aligned} \tag{12.80}$$

where

$$\begin{aligned}
Z &= G_{\text{M},i}^{(l)}/G_{\mu,i}, \\
X &= G_{\mu,i}^{(l)}/G_{\mu,i}, \\
Y &= G_{\text{M},i}^{(l)}/G_{\text{M},i}, \\
W &= G_{\mu,i}^{(l)}/G_{\text{M},i}\ , \quad 0 < Z, X, Y, W < 1.
\end{aligned} \tag{12.81}$$

Since each transmit branch has equal chance of being selected, the expected value of the total forward transmit power by each BS branch, given N' and M', is

$$\begin{aligned}
\text{E}[P_{\mu}^{\text{STD}}|N', M'] &= \frac{N'}{L} P_{\text{T}} \text{E}[P_{\mu,i}^{\text{STD}}|\text{MS}_i \in \text{microcell}] \\
&\quad + \frac{M - M'}{L} P_{\text{T}} \text{E}[P_{\mu,i}^{\text{STD}}|\text{MS}_i \in \text{macrocell}],
\end{aligned} \tag{12.82}$$

$$\begin{aligned}
\text{E}[P_{\text{M}}^{\text{STD}}|N', M'] &= \frac{N - N'}{L} P_{\text{T}} \text{E}[P_{\text{M},i}^{\text{STD}}|\text{MS}_i \in \text{microcell}] \\
&\quad + \frac{M'}{L} P_{\text{T}} \text{E}[P_{\text{M},i}^{\text{STD}}|\text{MS}_i \in \text{macrocell}].
\end{aligned} \tag{12.83}$$

The expectations $\text{E}[P_{\mu}^{\text{STD}}]$ and $\text{E}[P_{\text{M}}^{\text{STD}}]$ can now be computed as in (12.66) with the following Pr_{μ} and Pr_{M}:

$$\begin{aligned}
\text{Pr}_{\mu} &= \text{P}[\max[G_{\mu,i}^{(1)}, \cdots, G_{\mu,i}^{(L)}] > \max[G_{\text{M},i}^{(1)}, \cdots, G_{\text{M},i}^{(L)}]|\text{MS}_i \in \text{microcell}] \\
&= \text{P}[G_{\mu,i} > G_{\text{M},i}|\text{MS}_i \in \text{microcell}], \\
\text{Pr}_{\text{M}} &= \text{P}[G_{\text{M},i} > G_{\mu,i}|\text{MS}_i \in \text{macrocell}].
\end{aligned} \tag{12.84}$$

12.3.3.3 Numerical Results

Table 12.3 compares the analytical and simulation results of the single cell model. These results are obtained with $d_{\text{c}} = 692\,\text{m}$. The analytical results require less than

Table 12.3 Single cell model forward performance results

		Non-STD		STD, $L = 2$		STD, $L = 3$	
N	M	$\text{CIR}_{\text{anal.}}$ dB	$\text{CIR}_{\text{sim.}}$ dB	$\text{CIR}_{\text{anal.}}$ dB	$\text{CIR}_{\text{sim.}}$ dB	$\text{CIR}_{\text{anal.}}$ dB	$\text{CIR}_{\text{sim.}}$ dB
10	10	−11.54	−11.21	−9.99	−9.65	−9.31	−8.86
15	10	−12.80	−12.56	−11.25	−11.02	−10.57	−10.20
20	15	−14.19	−14.02	−12.64	−12.46	−11.96	−11.67
20	20	−14.56	−14.40	−13.01	−12.84	−12.34	−12.04

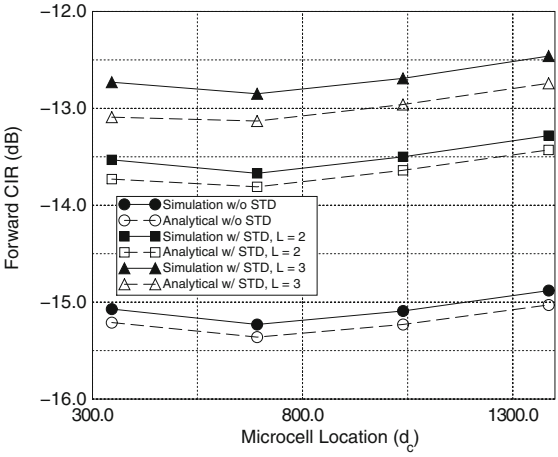

Fig. 12.16 Forward link performance for different microcell locations

15 iteration loops for the γs to converge. The analytical and simulation results are in good agreement, although the analytical results exhibit lower values than the simulation results. This due to the analytical interference assumption in (12.54) which results in a pessimistic interference level. However, the differences become marginal as the number of MSs increases. Table 12.3 also shows the results obtained with STD. Again, the analytical results closely follow the simulation results. One can immediately see the benefit of using STD on forward link performance. With two-branch transmit diversity the forward link CIR performance improves by 1.5 dB, and it improves by 2.5 dB with three-branch transmit diversity.

Figure 12.16 compares the analytical and simulation results as a function of the microcell location, d_c, while the system load is fixed at 24 MSs per cell. Again, they are in good agreement. The differences between the analytical and simulation results in the figure are larger for $L = 3$ than $L = 2$ due to the assumption in (12.72). But, the differences are still small considering they are within 0.3 dB.

Figure 12.17 shows the average forward link performance results obtained from the multicell model in Fig. 12.11 consisting of three macrocells and a cluster of three microcells. The benefit of STD is more evident from these results where the system benefits from the added diversity effect due to multiple cell locations. Although the performance varies slightly, STD effectively neutralizes the effect of the microcell

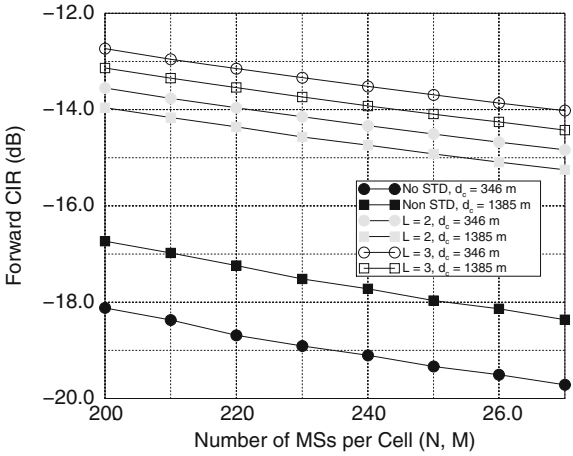

Fig. 12.17 Forward performance for the multicell model in Fig. 12.11

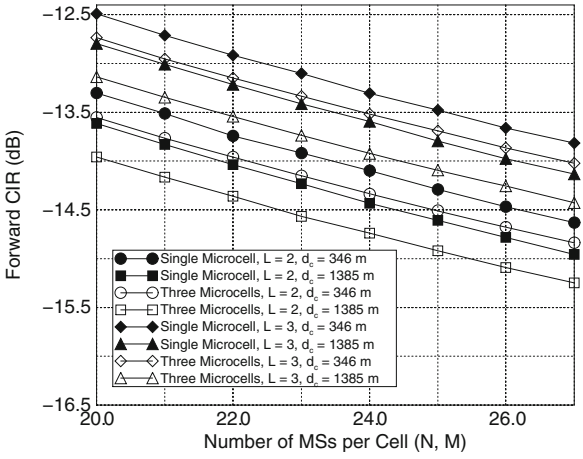

Fig. 12.18 Forward performance for different microcell cluster sizes

cluster location on forward performance. Without STD, the performance suffers if the cluster is located too close to a macrocell BS. From Fig. 12.17 we observe about 1.5 dB performance difference between the cluster locations, 346 and 1,385 m, without STD. One interesting observation is that performance improves slightly as d_c decreases with STD, which is opposite of what we observe in non-STD case. Although the cross interference between the hierarchical layers increases with smaller d_c, STD takes advantage of increased inter-layer diversity effect which ultimately results in improved performance.

Figure 12.18 shows the effect of the microcell cluster size on the forward link performance. The plot shows the performance comparison between a single cell cluster and a three-cell cluster. We have observed in the previous section that HMRC allows microcell(s) to be added without impacting the existing reverse link capacity. With STD, however, the forward link performance does depend on the microcell

cluster size, and an increase in the number of microcells in the cluster causes the performance to suffer. The added diversity effect is apparently not enough to fully compensate for increase in interference resulting from the microcell increase. However, the performance degradation is negligible considering the capacity gain obtained by adding microcell(s). For example, assuming the target CIR is set to -14 dB, a three-macrocell system with a single cell cluster has capacity of 26 MSs per cell at $d_c = 1{,}385$ m with $L = 3$. With the same exact setting, the same system with a three-cell cluster achieves 24 MSs per cell, yet its overall system capacity is far greater due to the added microcells.

From Figs. 12.12 and 12.17, we observe that a forward link performance comparable to the reverse link HMRC performance can be achieved by implementing STD with $L = 3$. Not only does STD improve the forward performance, but it can also benefit the reverse link performance by providing additional BS antenna elements for stronger combining.

Appendix 1: Derivation of Equation (12.75)

The conditional pdf of the link gain, G, is

$$p_{G|\Omega_p}(x) = \frac{2}{\Omega_p} e^{-x/\Omega_p}(1 - e^{-x/\Omega_p}). \tag{12.85}$$

Averaging over distribution of log-normal shadowing yields the composite pdf for squared envelope

$$p_G(g) = \int_0^\infty \frac{2}{\Omega_p} e^{-g/\Omega_p}(1 - e^{-g/\Omega_p}) \times \frac{1}{\sqrt{2\pi}\xi\sigma_\Omega\Omega_p} \exp\left\{ -\frac{\left(10\log_{10}\{\Omega_p\} - \mu_{\Omega_{p\ (\mathrm{dBm})}}\right)^2}{2\sigma_\Omega^2} \right\} d\Omega_p. \tag{12.86}$$

The mean of the approximate log-normal distribution is

$$\begin{aligned} \mu_{G\ (\mathrm{dBm})} &= E[10\log_{10}\{g\}] \\ &= \int_0^\infty \int_0^\infty (10\log_{10}\{g\}) \frac{2}{\Omega_p} e^{-g/\Omega_p}(1 - e^{-g/\Omega_p}) \\ &\quad \times \frac{1}{\sqrt{2\pi}\xi\sigma_\Omega\Omega_p} \exp\left\{ -\frac{\left(10\log_{10}\{\Omega_p\} - \mu_{\Omega_{p\ (\mathrm{dBm})}}\right)^2}{2\sigma_\Omega^2} \right\} dw d\Omega_p \end{aligned}$$

$$= \int_0^\infty \frac{1}{\sqrt{2\pi}\sigma_\Omega \xi^2 \Omega_\mathrm{p}^2} \exp\left\{ -\frac{\left(10\log_{10}\{\Omega_\mathrm{p}\} - \mu_{\Omega_\mathrm{p}\,(\mathrm{dBm})}\right)^2}{2\sigma_\Omega^2} \right\}$$

$$\times \int_0^\infty 2\ln(g) \mathrm{e}^{-g/\Omega_\mathrm{p}} \left(1 - \mathrm{e}^{-g/\Omega_\mathrm{p}}\right) \mathrm{d}g \mathrm{d}\Omega_\mathrm{p}. \tag{12.87}$$

From [118, 4.352.1], the inner integral becomes

$$\int_0^\infty 2\ln(g) \mathrm{e}^{-g/\Omega_\mathrm{p}} (1 - \mathrm{e}^{-g/w\Omega_\mathrm{p}}) \mathrm{d}g = \Omega_\mathrm{p}(\ln(2) + \ln(\Omega_\mathrm{p}) - C), \tag{12.88}$$

where $C \simeq 0.5772$ is Euler's constant. Hence,

$$\mu_{\mathrm{G}\,(\mathrm{dBm})} = \xi^{-1}(\ln(2) - C) + \mu_{\Omega_\mathrm{p}\,(\mathrm{dBm})}. \tag{12.89}$$

In a similar fashion, the mean square value is

$$\mathrm{E}[(10\log_{10}\{g\})^2] = \int_0^\infty \int_0^\infty (10\log_{10}\{g\})^2 \frac{2}{\Omega_\mathrm{p}} \mathrm{e}^{-g/\Omega_\mathrm{p}} (1 - \mathrm{e}^{-g/\Omega_\mathrm{p}})$$

$$\times \frac{1}{\sqrt{2\pi}\sigma_\Omega \xi \Omega_\mathrm{p}} \exp\left\{ -\frac{\left(10\log_{10}\{\Omega_\mathrm{p}\} - \mu_{\Omega_\mathrm{p}\,(\mathrm{dBm})}\right)^2}{2\sigma_\Omega^2} \right\} \mathrm{d}g \mathrm{d}\Omega_\mathrm{p}$$

$$= \int_0^\infty \frac{1}{\sqrt{2\pi}\sigma_\Omega \xi^3 \Omega_\mathrm{p}^2} \exp\left\{ -\frac{\left(10\log_{10}\{\Omega_\mathrm{p}\} - \mu_{\Omega_\mathrm{p}\,(\mathrm{dBm})}\right)^2}{2\sigma_\Omega^2} \right\}$$

$$\times \int_0^\infty 2(\ln g)^2 \mathrm{e}^{-g/\Omega_\mathrm{p}} (1 - \mathrm{e}^{-g/\Omega_\mathrm{p}}) \mathrm{d}g \mathrm{d}\Omega_\mathrm{p}. \tag{12.90}$$

From [118, 4.358.2], the inner integrals become

$$\int_0^\infty 2(\ln g)^2 \mathrm{e}^{-g/\Omega_\mathrm{p}} \mathrm{d}g = 2\Omega_\mathrm{p}\Big((\ln \Omega_\mathrm{p} - C) + \zeta(2,1) \Big),$$

$$\int_0^\infty (\ln g)^2 \mathrm{e}^{-2g/\Omega_\mathrm{p}} \mathrm{d}g = \Omega_\mathrm{p}\Big((\ln \Omega_\mathrm{p} - \ln(2) - C)^2 + \zeta(2,1) \Big), \tag{12.91}$$

where

$$\zeta(2,m) = \sum_{k=0}^{\infty} \frac{1}{(m+k)^2} \tag{12.92}$$

is Reimann's zeta function. Finally, the variance is

$$\begin{aligned}\sigma^2_{\mathrm{G\ (dBm)}} &= \mathrm{E}[(10\log_{10}\{g\})^2] - \mathrm{E}^2[10\log_{10}\{g\}] \\ &= \xi^{-2}\Big(\zeta(2,1) - 2(\ln 2)^2\Big) + \sigma^2_{\Omega}. \end{aligned} \tag{12.93}$$

Appendix 2: Derivation of Equation (12.76)

For $L = 3$, the mean of log-normal approximation is

$$\begin{aligned}\mathrm{E}[10\log_{10}\{g\}] &= \int_0^{\infty}\int_0^{\infty} 10\log_{10}\{g\}\frac{3}{\Omega_{\mathrm{p}}}\mathrm{e}^{-g/\Omega_{\mathrm{p}}}(1-\mathrm{e}^{-g/\Omega_{\mathrm{p}}})^2 \\ &\quad\times\frac{1}{\sqrt{2\pi}\xi\,\sigma_{\Omega}\Omega_{\mathrm{p}}}\exp\left\{-\frac{\Big(10\log_{10}\{\Omega_{\mathrm{p}}\} - \mu_{\Omega_{\mathrm{p}}\ (\mathrm{dBm})}\Big)^2}{2\sigma^2_{\Omega}}\right\}\mathrm{d}g\mathrm{d}\Omega_{\mathrm{p}} \\ &= \int_0^{\infty}\frac{1}{\sqrt{2\pi}\xi^2\sigma_{\Omega}\Omega^2_{\mathrm{p}}}\exp\left\{-\frac{\Big(10\log_{10}\{\Omega_{\mathrm{p}}\} - \mu_{\Omega_{\mathrm{p}}\ (\mathrm{dBm})}\Big)^2}{2\sigma^2_{\Omega}}\right\} \\ &\quad\times\int_0^{\infty} 3\ln(g)(\mathrm{e}^{-g/\Omega_{\mathrm{p}}} - 2\mathrm{e}^{-2g/\Omega_{\mathrm{p}}} + \mathrm{e}^{-3/\Omega_{\mathrm{p}}})\mathrm{d}g\mathrm{d}\Omega_{\mathrm{p}}. \end{aligned} \tag{12.94}$$

Using [118, 4.352.1]

$$\int_0^{\infty} 3\ln(g)(\mathrm{e}^{-g/\Omega_{\mathrm{p}}} - 2\mathrm{e}^{-2g/\Omega_{\mathrm{p}}} + \mathrm{e}^{-3/\Omega_{\mathrm{p}}})\mathrm{d}g = \Omega_{\mathrm{p}}(3\ln(2) - \ln(3) - C + \ln(\Omega_{\mathrm{p}})) \tag{12.95}$$

and, therefore,

$$\mu_{\mathrm{G\ (dBm)}} = \mathrm{E}[10\log_{10}\{g\}] = \xi^{-1}(3\ln(2) - \ln(3) - C) + \mu_{\Omega_{\mathrm{p}}\ (\mathrm{dBm})}. \tag{12.96}$$

Similarly, the second moment of the approximation is

$$\begin{aligned}\mathrm{E}[(10\log_{10}\{g\})^2] &= \int_0^{\infty}\int_0^{\infty} (10\log_{10}\{g\})^2\frac{3}{\Omega_{\mathrm{p}}}\mathrm{e}^{-g/\Omega_{\mathrm{p}}}(1-\mathrm{e}^{-g/\Omega_{\mathrm{p}}})^2 \\ &\quad\times\frac{1}{\sqrt{2\pi}\sigma_{\Omega}\xi\,\Omega_{\mathrm{p}}}\exp\left\{-\frac{\Big(10\log_{10}\{\Omega_{\mathrm{p}}\} - \mu_{\Omega_{\mathrm{p}}\ (\mathrm{dBm})}\Big)^2}{2\sigma^2_{\Omega}}\right\}\mathrm{d}g\mathrm{d}\Omega_{\mathrm{p}} \end{aligned}$$

$$= \int_0^\infty \frac{1}{\sqrt{2\pi}\sigma_\Omega \xi^3 \Omega_\mathrm{p}^2} \exp\left\{ -\frac{\left(10\log_{10}\{\Omega_\mathrm{p}\} - \mu_{\Omega_\mathrm{p}\ (\mathrm{dBm})}\right)^2}{2\sigma_\Omega^2} \right\}$$

$$\times \int_0^\infty 3(\ln(g))^2 (\mathrm{e}^{-g/\Omega_\mathrm{p}} - 2\mathrm{e}^{-2g/\Omega_\mathrm{p}} + \mathrm{e}^{-3/\Omega_\mathrm{p}}) \mathrm{d}g \mathrm{d}\Omega_\mathrm{p}. \quad (12.97)$$

Using [118, 4.358.2]

$$\int_0^\infty 3(\ln(g))^2 (\mathrm{e}^{-g/\Omega_\mathrm{p}} - 2\mathrm{e}^{-2g/\Omega_\mathrm{p}} + \mathrm{e}^{-3/\Omega_\mathrm{p}}) \mathrm{d}g = \Omega_\mathrm{p} \Big(-6C\ln(2) + 6(2)\ln(\Omega_\mathrm{p})$$

$$-3(\ln(2))^2 + C^2 - 2C\ln(\Omega_\mathrm{p})$$

$$+(\ln(\Omega_\mathrm{p}))^2 + 2C\ln(3)$$

$$-2\ln(3)\ln(\Omega_\mathrm{p}) + (\ln(3))^2$$

$$+\zeta(2,1)\Big) \quad (12.98)$$

and, therefore,

$$\mathrm{E}[(10\log_{10}\{g\})^2] = \xi^{-2}\Big(-6C\ln(2) - 3(\ln(2))^2 + C^2$$

$$+2C\ln(3) + (\ln(3))^2 + \zeta(2,1)\Big)$$

$$+6\ln(2)\mu_{\Omega_\mathrm{p}\ (\mathrm{dBm})} - 2C\mu_{\Omega_\mathrm{p}\ (\mathrm{dBm})} - 2\ln(3)\mu_{\Omega_\mathrm{p}\ (\mathrm{dBm})}$$

$$+\sigma_\Omega^2 + \mu_{\Omega_\mathrm{p}\ (\mathrm{dBm})}^2. \quad (12.99)$$

Therefore, the variance of the log-normal approximation is

$$\sigma_{\mathrm{G}\ (\mathrm{dBm})}^2 = \mathrm{E}[(10\log_{10}\{g\})^2] - \mu_{\mathrm{G}\ (\mathrm{dBm})}^2$$

$$= \xi^{-2}\Big(\zeta(2,1) - 12(\ln(2))^2 + 6\ln(2)\ln(3)\Big) + \sigma_\Omega^2. \quad (12.100)$$

Problems

12.1. Consider a CDMA cellular system where there are five in-cell interferers. Each interferer is independently active with probability p, and is characterized by a power control error ς_{E_j}. The power control errors, ς_{E_j} (in dB) are independent zero-mean Gaussian random variables with variance σ_{E}^2. Hence, the in-cell interference is

$$I_{\mathrm{in}} = C \sum_{j=1}^{5} 10^{\varsigma_{\mathrm{E}_j}/10} \chi_j,$$

where

$$\chi_j = \begin{cases} 1 & \text{with probability } p, \\ 0 & \text{with probability } 1-p. \end{cases}$$

(a) The in-cell interference can be approximated as a log-normal random variable conditioned on the number of active interferers

$$k = \sum_{j=1}^{5} \chi_j.$$

Determine the mean and variance of the log-normal approximation as a function of k for $\sigma_{\mathrm{E}} = 1$, 2, and 3 dB. Use the Fenton–Wilkinson approach.

(b) Assuming that the value of $(I_{\mathrm{in}})_{\mathrm{dB}}$ is Gaussian when conditioned on the number of active interferers, write down and expression for the pdf of $(I_{\mathrm{in}})_{\mathrm{dB}}$.

12.2. (**Computer exercise**) The purpose of this problem is to determine the relative contribution of the first-, second- and third-tier cells to the out-of-cell interference in a CDMA cellular system. Also, we wish to determine the impact of the path loss exponent on the out-of-cell interference.

Consider a CDMA cellular system characterized by log-normal shadowing with a shadow standard deviation σ_Ω dB and inverse β power path loss. Neglect envelope fading. All other factors such as base-station antenna heights, cell sizes, etc. are uniform. The ratio of the mean out-of-cell interference to mean in-cell interference is

$$\theta = \frac{\mathrm{E}[I_{\mathrm{o}}/C]}{pK},$$

where

$$\mathrm{E}[I_{\mathrm{o}}/C] = p \int\int \exp\left\{ \frac{\xi^2 \sigma_x^2}{2} + \xi \mu_x \right\} \left(1 - Q\left(-\xi \sigma_x - \frac{\mu_x}{\sigma_x} \right) \right) \rho \, \mathrm{d}A$$

and

$$\mu_x = \mu_{i0} - \mu_{ij},$$
$$\sigma_x^2 = 2\sigma_\Omega^2.$$

For regular hexagonal cells, the subscriber density is

$$\rho = \frac{2K}{3\sqrt{3}R^2}.$$

Hence,

$$\theta = \frac{2}{3\sqrt{3}R^2} \int\int \exp\left\{\frac{\xi^2\sigma_x^2}{2} + \xi\mu_x\right\}\left(1 - Q\left(-\xi\sigma_x - \frac{\mu_x}{\sigma_x}\right)\right)\rho \mathrm{d}A,$$

where the double integral is over the two-dimensional out-of-cell area.

(a) Consider the first tier of interfering cells. For the case of $\sigma_\Omega = 8$ dB, calculate θ when $\beta = 3$ and $\beta = 4$.
(b) Repeat part (a), but this time consider only the *second* tier of interfering cells.
(c) Finally, repeat part (a), for the *third* tier of interfering cells.
(d) What conclusions can you draw?

12.3. CDMA systems use soft handoff, where the transmissions to/from multiple BSs are combined to give a macro-diversity advantage. Suppose that the receive bit energy-to-noise ratio for branch i, denoted by γ_i, has the probability density

$$p_{\gamma_i}(x) = \frac{1}{\bar{\gamma}_i} \mathrm{e}^{-x/\bar{\gamma}_i},$$

where $\bar{\gamma}_i = \mathrm{E}[\gamma_i]$.

(a) The reverse link uses selection macro-diversity such that

$$\gamma_\mathrm{b}^\mathrm{s} = \max\{\gamma_1, \gamma_2, \ldots, \gamma_L\}.$$

An outage occurs if $\gamma_\mathrm{b}^\mathrm{s} < \gamma_\mathrm{th}$. What is the probability of outage?
(b) The forward link uses maximal ratio combining such that

$$\gamma_\mathrm{b}^\mathrm{mr} = \gamma_1 + \gamma_2 + \cdots + \gamma_L.$$

Again, an outage occurs if $\gamma_\mathrm{b}^\mathrm{mr} < \gamma_\mathrm{th}$. What is the probability of outage if $\bar{\gamma}_1 = \bar{\gamma}_2 = \cdots = \bar{\gamma}_L$?
(c) For $L = 2$ and an outage probability of 10^{-4} what is the *difference* in the required γ_th (in units of decibels) with selection and maximal ratio combining, again assuming that $\bar{\gamma}_1 = \bar{\gamma}_2$?